Electrocatalytic Performance of NiNH2BDC MOF Based Composites with rGO For Methanol Oxidation Reaction

Lubna Yaqoob
National University of Sciences and Technology
Tayyaba Noor (tayyaba.noor@scme.nust.edu.pk)
National University of Sciences and Technology
Naseem Iqbal
National University of Sciences and Technology
Habib Nasir
National University of Sciences and Technology
Asad Mumtaz
National University of Sciences and Technology

Research Article

Keywords: Electrocatalysts, Methanol oxidation reaction, Hydrogen Production, Reduced graphene oxide, Metal organic frameworks

Posted Date: April 6th, 2021

DOI: https://doi.org/10.21203/rs.3.rs-374530/v1

Electrocatalytic performance of $NiNH_2BDC$ MOF based composites with rGO for methanol oxidation reaction

LubnaYaqoob[1], Tayyaba Noor*[2], Naseem Iqbal[3], Habib Nasir[1], Asad Mumtaz[1]

[1]School of Natural Sciences (SNS), National University of Sciences and Technology (NUST), Islamabad, Pakistan

[2]School of Chemical and Materials Engineering (SCME), National University of Sciences and Technology (NUST), Islamabad, Pakistan

[3]U.S-Pakistan Center for Advanced Studies in Energy (USPCAS-E), National University of Sciences and Technology (NUST), H-12 Campus, Islamabad 44000, Pakistan.

*Corresponding Author: Tel: +92 51 9085 5121, Email: tayyaba.noor@scme.nust.edu.pk.

Abstract

Present work comprehensively investigated the electrochemical response of Nickel-2 Aminoterephthalic acid metal organic framework ($NiNH_2BDC$) and its reduced graphitic carbon (rGO) based hybrids for methanol (CH_3OH) oxidation reaction (MOR) in an alkaline environment. In thorough analysis of solvothermally synthesized Metal-organic frameworks (MOFs) and its reduced graphitic carbon based hybrids, functional groups detection was performed by FTIR, morphological study by SEM, crystal structure analysis via XRD, and elemental analysis through XPS while electrochemical testing was accomplished by chronoamperometry (CA), cyclic voltametric method (CV), electrochemically active surface area (EASA), Tafel slope (b), Electron

impedance spectroscopy (EIS), mass activity, and roughness factor. Among all the fabricated composites, NiNH_2BDC MOF/5 wt % rGO hybrid by possessing auspicious current density (j) of 267.7 mA / cm^2 at 0.699 V (vs Hg/HgO), a Tafel slope value of 60.8 $mV.dec^{-1}$, EASA value of 15.7 cm^2, and by exhibiting resistance of 13.26 Ω in a 3 M CH_3OH / 1M NaOH solution displays grander electrocatalytic activity as compared to state-of-the-art platinum-based electrocatalysts.

Keywords: Electrocatalysts; Methanol oxidation reaction; Hydrogen Production; Reduced graphene oxide; Metal organic frameworks

1.0. Introduction

At present, amongst the top ten problems of humanity, the sternest encountered problem is the energy predicament due to prompt and emergent worldwide energy demands and immense combustion of fossil fuels (non-renewable energy sources). The invention and development of renewable, green, and economical energy sources to handle the limitations of conventional energy-producing and transforming means for a sustainable future is the field of attention and investigation for scientists and researchers of the 21st century [1-5]. Fuel cells due to their smooth functioning, pronounced energy density, and non-polluting products are emergent, immaculate, green and dynamic replacement of traditional fossil fuels. Amongst the multiple fuel cells, direct CH_3OH fuel cell (DMFC) is the prospective candidate for handy devices and light-duty vehicles owing to prerequisite low temperature, liquid nature of fuel, quick refueling, eminent power density, facile charging, and minimum environmental influence [6-15]. Furthermore, H_2 being a major product of the CH_3OH oxidation process in DMFC is also a sustainable and pollution-free energy source due to its pronounced energy density, elevated combustion efficiency, as well as storable and renewable nature and it is converted to water during oxidation reaction by excluding carbon imprint [16, 17].

The complete oxidation process with E^0 values vs RHE is represented as follows: [18].

$CH_3OH + H_2O \rightarrow CO_2 + 6H^+ + 6e^-$ $E^0 = 0.016V$ (Anodic reaction)

$3/2\ O_2 + 6H^+ + 6e^- \rightarrow 3H_2O$ $E^0 = 1.229\ V$ (Cathodic reaction)

$CH_3OH + 3/2\ O_2 \rightarrow CO_2 + 2H_2O$ $E^0 = 1.213\ V$ (Overall reaction)

Conversely, methanol cross over (depressed redox process), high manufacturing cost, catalyst inactivation by reaction intermediates(CO, CHO, etc), sluggish kinetics owing to intricate six electron oxidation process (high overpotential), and utilization of expensive noble metal-based catalysts are the main obstacles in a direct methanol fuel cell commercialization. So, the development of a most appropriate and low-cost electrocatalyst with an outstanding tendency of complete oxidation of CH_3OH is an imperative requirement of a direct methanol fuel cell [19-21]. At present, state-of-the-art platinum-based electrocatalysts due to their accelerated electron movement toward CH_3OH and unique electronic arrangement are the most proficient electrocatalysts in DMFCs [6,7]. However, the main problems related with limited platinum exploitation are (a) high cost (b) destabilization in an acidic media (c) catalyst inactivation by reaction intermediates predominantly CO, and (d) dejected electrocatalytic activity due to less exposed electroactive sites. Pt alloys with transition elements (Fe, Ni, Co, etc) and with comparatively less costly metals (Ru, Pd, Ir, etc), in-situ reactivation process and composites of Pt by using CB (carbon black), CNTs (carbon nanotubes), GO (graphene oxide), and rGO (graphene oxide in reduced form) are the most promising solutions of above-mentioned problems and results in improved electrocatalytic activity. Pt surface poisoning and cost issues can be mitigated by doping of stable and corrosion-resistant IrO_2 in Pt. Likewise, doping of appropriate amount of Ru into Pt-based catalysts expedite the liberation of adsorbed OH^- for rapid oxidation of CO to CO_2,

minimize the Pt poisoning, and give consequent high electrocatalytic activity. Moreover, transition metal-based oxides, carbides, nitrides, borides, as well as double layered hydroxides (LDH) are also embryonic materials with a tremendous performance for the methanol oxidation process [22-25]. Pt inactivation in an acidic media due to deposition of impurities (already present metals) can be lessened by switching the electrolyte polarity (reactivation process) under optimized conditions without any compromise on stability and dissolution of electrolyte and maximum removal of impurities. Furthermore, in basic media, easy CO oxidation, facile availability of OH^-, and greater stability of material lead to enhanced electrocatalytic response [26, 27].

From the prior few decades, coordination polymers (MOFs) based electrocatalysts are the area of interest for researchers to use them as a favorable alternative of expensive rare earth metal encompassing catalyst of MOR in an alkaline environment.

Metal organic frameworks are crystalline and porous bodies prepared by linking of metal node and polydendate ligand to develop a one dimensional to three dimensional structures. Their less density, gigantic surface area, porosity, tunable, and stable nature make it possible to effectively utilize them for drug transport, sensing, storage and ablution of gases, water decontamination, batteries, supercapacitors, as well as for catalytic reactions in a fuel cell [28-30].

In the case of MOFs ; (1) facile synthesis of MOFs (2) low cost and abundance of precursors (3) porosity leading to smooth diffusion process (4) exalted conductivity along with thermal and chemical stability (5) active metal sites (6) enriched reactants adsorption, and (7) huge surface area proposed them as a suitable alternative of expensive noble metals [31]. Moreover, in nickel-based MOFs (a) easy access to economical precursors (b) variable valency of Ni metal (+1 to + 3), predominantly higher oxidation state (c) formation of nickel oxides and hydroxides on the surface,

and (d) conversion of $Ni(OH)_2$ (β) → NiOOH (β) → NiOOH (γ) during electrochemical testing all are responsible for excellent electrocatalytic response [32-34].

Furthermore, MOFs composites with conductive carbonaceous materials such as graphene, oxidized form of graphene (GO), reduced form of graphene oxide (rGO), porous carbon black, and carbon nanotubes (CNTs) show improved electrocatalytic behavior due to the following reasons; (a) enhanced stability due to hydrophobic sp^2 carbon domain (b) upsurge conductivity due to -ve inductive effect of carbon-based materials (c) restricted agglomeration owing to MOFs NPs ultrafine dissipation on the support surface leading to faster kinetics (d) multiple continuous channels expediting the charge transport process (e) huge surface area provided by carbon-based support, and (f) metal active sites-carbonaceous support strong interaction (synergistic effect) accompanied with less resistance, smooth electrolyte diffusion and rapid electron transfer [35-38].

Li et al. in 2018 deposited metal (Pt-Ni) nanoparticles on spongy nickel frameworks surface by electrochemical activation technique. Pt/p-Ni nanoparticles with the almost double electrochemically active surface area in comparison to Pt/C composite exhibit improved CH_3OH oxidation activity as well as stability due to the following logics; (a) geometrical and electrical modification of Pt structure due to Ni (b) high CO tolerance due to strong chemical bonding between two metals (c) high surface area with plenty of exposed electroactive sites due to homogenous distribution of 4.34 nm-sized Ni-Pt alloy nanoparticles (d) effective utilization of active sites due to electrolyte in-depth percolation and (e) a porous structure with facile mass transfer [39].

Pt-Ni/C MOR electrocatalyst was prepared by Ortega and colleagues in 2018 via a facile impregnation method. The morphology and structural characterization techniques confirm the presence of double metals, reduction in particle size of Pt due to Ni inclusion, and huge surface

area. Furthermore, the formation of metal oxides and hydroxides and reformed electronic structure due to synergistic effect minimizes the CO adsorption and hasten the charge transfer process during the anodic process [40].

Ferrer and collaborators in 2018 manufactured nanocomposites of Pt with reduced form of graphene oxide and nanostructured carbon (NC) via embryonic wet impregnation method and did a comparative analysis of a sample with Pt/C by providing identical circumstances. The decreasing order of current density response was Pt/NC (355 $mA.mg^{-1}$) > Pt/rGO (332 $mA. mg^{-1}$) > Pt/C (180 $mA.mg^{-1}$). The enhanced electron transport at the electrode-electrolyte intersection along with hierarchal structure are the main reasons for improved electrochemical activity [41].

Li and associates in 2018 used the concept of H_2 reduction method to introduce an innovative Pt/ Ni_2P/CNTs complex electrocatalyst with low cost. The reduction in particle size, as well as their fine dispersion on carbon nanotubes (CNTs) surface after Ni_2P incorporation was mainly responsible for enhanced MOR performance of Pt NPs. An optimized sample with 6 % Ni_2P (Pt / 6% Ni_2P/CNTs) demonstrates more than twice of current density response than Pt/C-JM. Moreover, the high current density at onset potential and stable current response are the protuberant features of the reported sample in an alkaline media [42].

Surfactant assisted co-reduction approach was instigated by Li et al. to formulate bimetallic Ni-Sn nanoparticles (NPs) with precise size (3-5 nm) and composition in 2018. A Ni-Sn-based catalyst with high nickel content outweighs the methanol oxidation performances of simple Ni containing electrocatalyst. Carbon black supported Ni-Sn NPs delivers 0.05 A/cm^2 current density (j) at 1660 mV and show stable current response with little variation till 5000 seconds. The stimuli for this splendid performance were (a) modified electronic structure (b) inhibited nickel surface poising

effect due to oxidation of side product to CH_3OH, and (c) weak binding of reaction intermediates [43].

Askari and colleagues engendered a ternary metal sulfides/graphene composite (MoNiCoS/GO) through a one-step hydrothermal route (2018) and tried for the CH_3OH oxidation process under basic conditions. The ensuing MoNiCoS/GO electrocatlyst displays appropriate electrocatalytic behavior as well as ample diffusion current reflected by exchange current density calculation. Electrochemical testing proves that graphene is responsible for a large number of electroactive sites and conductive nature while two metals (Ni & Co) increase the surface effectiveness and facilitate the smooth electron transport process [44].

Nickel comprising MIL-110 MOR anode electrocatalyst reported by Wang and collaborators in 2019 was prepared by wet impregnation technique. Ni@MIL-110 electrocatalyst exhibits fine metal NPS dispersal plus massive surface area. Conversely, extreme nickel concentrations devastate the crystal structure. Cyclic voltammetry (CV) and stability testing represent the good CH_3OH oxidation activity of material in an alkaline environment [45].

A Ni MOF-based series reported by Noor et al. in 2019 was of NiO-MOF@rGO composites. Solvothermally prepared distorted NPs of NiO-MOF / 5 wt % rGO composite possesses low resistance and Tafel slope, high diffusion coefficient with minimum loss of current even after 60 minutes. [23].

A novel nickel-based anode catalyst (Ni_9S_8-C), fabricated by Hussain and associates (2019) through facile, low cost, and single-pot synthetic scheme to get paramount pure mixed-metal sulfide catalyst was examined for MOR. The resultant, Ni_9S_8 delivers the current density of 0.052 $A.cm^{-2}$ because of strong binding between nanoparticles and carbon substrate. Moreover, little

loss of current density even after 5000 seconds and minimum resistance authenticate the catalyst good response towards MOR [46].

Hydrothermally synthesized Nickel-Zinc layered double hydroxides were subsequently calcined by Wei et al. to get flower-like 3D microspheres of $Ni_{0.6}Zn_{0.4}O$. The tested sample with good reactants connection, enormous surface area, as well as swift electrons transfer due to zinc fusion show high anodic current (~0.053 A /cm^2), lowest Tafel slope (61.24 mV/dec), and long term stability for 36,000 seconds in a basic medium [47].

Hosseini and colleagues in 2019 conveyed the utmost nanostructured film of ZIF-8 at the oil- water interjunction, synthesized by a facile process at ambient conditions. The current density response of the sample (32.7mA/cm^2) for the CH_3OH oxidation process was better in comparison to Co-MOF-7, Pt film, Ni/ZIF-8, and Pd/ZIF. Moreover, minimal poisoning of ZIF-8 film (0.1 %) accompanied with power density of (15.4 mW/cm^2) validate the good electrocatalytic response of material for CH_3OH oxidation process [48].

In 2019, Jian et al. illustrated the efficiency and stability of trimetallic nano alloy of PtNiCu towards CH_3OH oxidation process at low pH and observed that the introduction of an infinitesimal quantity of Ni in Pt-Cu alloy enhances its electrocatalytic application for MOR. An optimized $Pt_{60}Ni_3Cu_{37}$ catalyst with forward current of 1.3 A/mg at 1.73 V (vs RHE) and 12 % current loss in chronoamperometry test shows better efficiency than porous $Pt_{55}Cu_{45}$ and Pt black [49].

MoS_2@CoNi-ZIF with MoS_2 perimeter around hollow Co-Ni ZIF nanomaterials was acquired by Liu and colleagues in 2019 by stirring followed by sonication technique at ambient conditions. Amongst the tested samples, a good oxidation response was shown by MoS_2@CoNi-ZIF as it delivers an anodic current of 9 mA /cm^2 on 1.40 V (vs RHE). Three considerable advantages of a resultant electrocatalyst are ; (i) bifunctional electrocatalytic response for MOR and H_2O splitting

process (ii) simple synthetic scheme without any further processing (iii) pronounced stability as a result of robust synergistic effect among MoS_2, CoNi-ZIF and metal oxides [50].

Yaqoob et al. in 2019 fabricated Ni-BTC MOF/1-5 wt % rGO composites for MOR in an alkaline condition. Solvothermally fabricated Ni-BTC MOF/reduced graphitic carbon composites possess hexagonal shape complemented with peaked surface area, good stability, and boosted conductivity as a result of rGO incorporation. Among the synthesized samples, Ni-BTC/4 wt % rGO composite delivers a forward current of 0.20 A/cm^2 at 1.614 V (vs RHE), possess lowest Tafel slope (0.08 $V.dec^{-1}$), minimum capacitance (18.12 Ω), and long term stability for 3600 seconds. Furthermore, product analysis confirms the oxidation of methanol to formic acid with 62 % conversion efficiency [51].

Stephanie and colleagues (2016) adopted a facile multistep synthetic process at ambient conditions to report Fe-Ni NPs as a MOR catalyst. During the reaction, the Fe (core)-Ni (shell) nanoparticles show the oxidation of Ni shell to α-Ni $(OH)_2$ (major contribution) and β-NiOOH (minor contribution) and formation of metallic nanoparticles as well. During methanol concentration optimization, direct relationship of a current density with methanol concentration was observed. The tested sample provides the forward current density (j_f) of 0.048 A/cm^2 at anodic potential of 1.58 V (vs RHE) [52].

In this study, solvothermally fabricated $NiNH_2BDC$ MOF/1, 2, 5 wt % reduced form of graphene oxides hybrids ($NiNH_2BDC$/ rGO) were thoroughly analyzed for CH_3OH oxidation process in 1M NaOH solution. In MOF/rGO composites diverse aspects for instance; (a) availability of manifold Ni oxidation states ; +2 to +3, smoothened redox process via facile electron movement (b) coordination compound formation propensity of nickel (c) development of defects and vacancies (d) rGO sheets tremendous stability and conductivity (e) escalated surface area of MOF (f) MOF

NPs homogenous dispersal on the surface of support, and (g) synergistic effect between rGO and MOF, all support the incredible enactment of as-synthesized materials for methanol oxidation reaction. According to our literature survey, the catalytic tendency of NiNH_2BDC MOF/1, 2, 5 wt % reduced graphene oxide hybrids for CH_3OH oxidation process has not been conveyed in the literature to date.

2.0. Experimental Section

99 % pure reagents and chemicals without further treatment were utilized for synthesis. Prerequisite chemicals for the fabrication purpose include Ni $(NO_3)_2.6H_2O$, 2-Aminoterephthalic acid (NH_2BDC), potassium permanganate ($KMnO_4$), sodium nitrate ($NaNO_3$) which were procured from Sigma Aldrich while Dimethylformamide (DMF), hydrazine hydrate, hydrogen peroxide, and sulphuric acid were picked up from Merck.

2.1. Fabrication of Ni NH_2BDC MOF

Synthesis of NiNH_2BDC MOF was carried out by an already described solvothermal methodology after slight modification [53]. 1 mmole solution of both of Ni $(NO_3)_2.6H_2O$ and 2-Aminoterephthalic acid in 15 ml DMF were prepared simply by stirring with subsequent slow mixing of Ni nitrate clear solution in linker solution. The homogenous mixture of MOF precursors acquired after one-hour stirring was drizzled to a 23 ml capacity autoclave (Teflon lined) and retained for twenty four hours at 393 K in an electric oven. After reaction accomplishment, the room temperature was attained by slow cooling of autoclave. Light green powdered material was achieved after repetitive washing of autoclave product with DMF and ethanol via centrifugation and vacuum drying at 348 K for 24 hours.

2.2. Fabrication of GO and rGO

Reported Hummer's method was utilized for GO Synthesis while rGO was synthesized through reduction of GO by hydrazine hydrate via 24 hours reflux at 373 K [54, 55].

2.3. Fabrication of Ni NH_2BDC MOF/rGO Composites

A NiNH_2BDC MOF/rGO hybrids (MOR catalyst) series was prepared by following the above-stated procedure. A clear solution of MOF obtained by the above-mentioned scheme and appropriate amount rGO were sonicated for two hours to acquire a uniform blend and then transmitted to stainless steel autoclave with Teflon inner cavity for 24 hours reaction at 393 K. A dry solid product was obtained after 3-4 times washing with DMF/ethanol via centrifugation followed by 24 hours vacuum drying at 348 K (Figure 1).

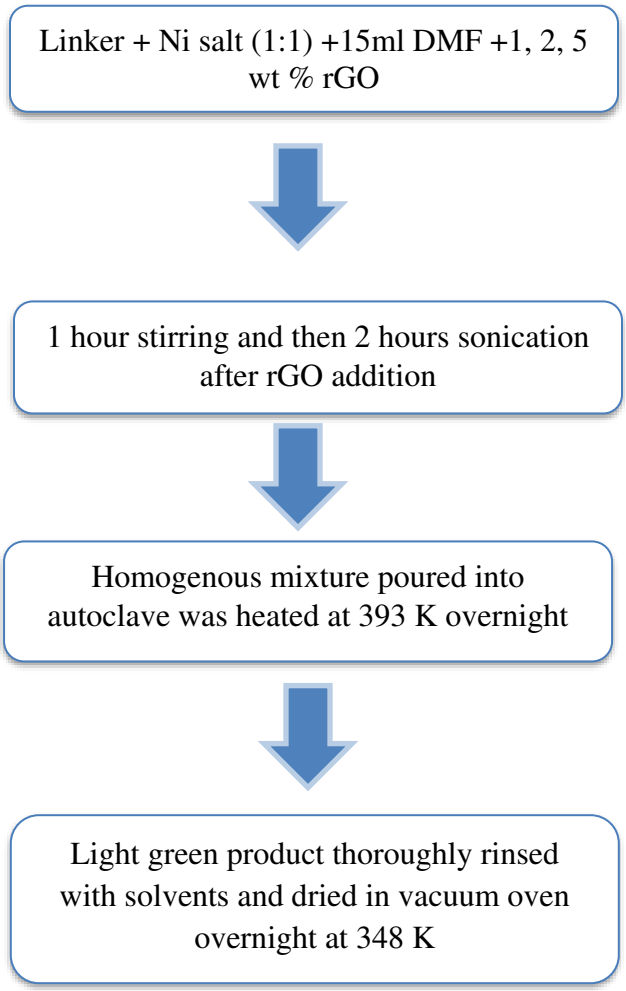

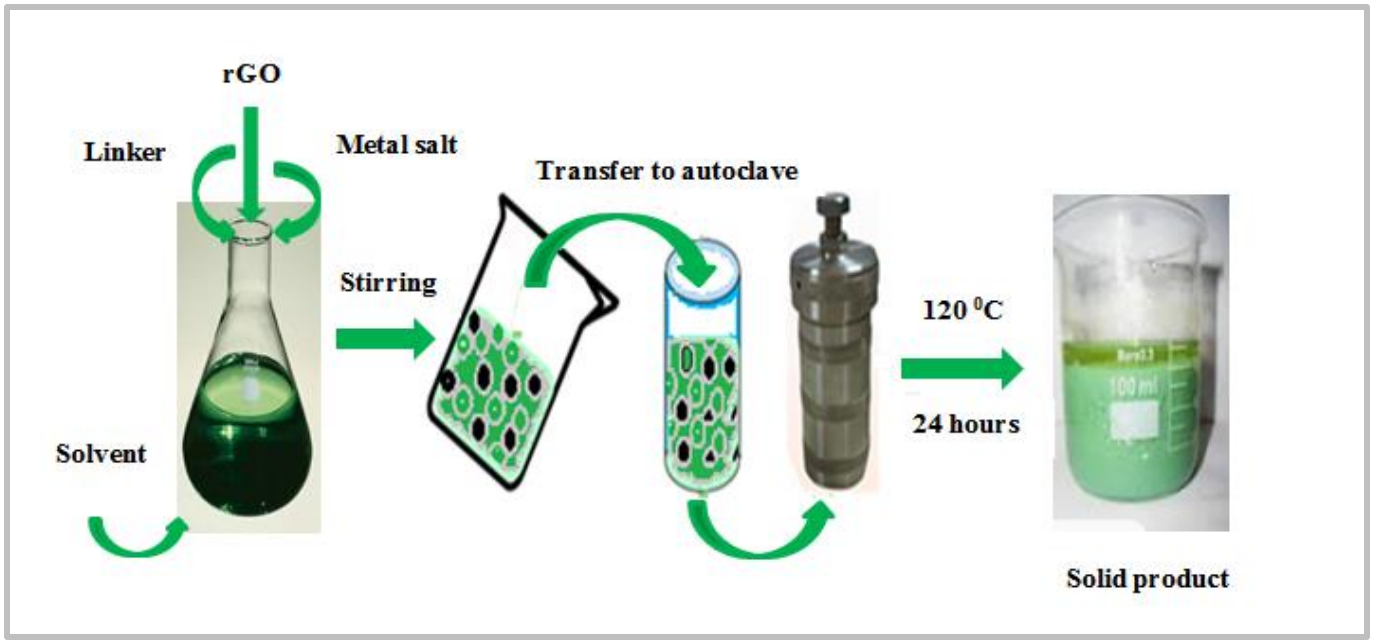

Figure 1. Stepwise synthetic scheme of $NiNH_2BDC$ MOF /1, 2, 5 wt % reduced graphitic carbon hybrids and flow sheet diagram for the synthesis of $NiNH_2BDC$ MOF/1, 2, 5 wt % reduced graphitic carbon hybrids.

2.4. Materials Characterization

For comprehensive characterization of as-synthesized samples, a Scanning electron microscope (VEGA 3 TESCAN) employed for exterior structure and morphology analysis. X-ray powder diffractometry (STOE Germany) was implemented for phase purity and crystalline nature scrutinization (Kα = Cu radiation, 0.1.54 ^{0}A, scanning range = 5^o – 80^o, step size = 4^o/s at 5 mA and 20 kV) while validation of functional groups and metal-ligand strong interaction was corroborated through FTIR spectrophotometer (Perkin spectrum) by selecting wavenumber range of 500-4000 cm^{-1}. Binding energy and composition records were collected by XPS (MI-600) respectively. The degree of defects and graphitization, as well as extent of crystallinity was ascertained via Raman Spectroscopy.

2.5. Electrocatalytic Measurements

An inclusive electrochemical evaluation was done in 3M CH_3OH/1 M NaOH mixture through the Gamry apparatus (Ref 3000 /3000 AE). To get homogenous ink of electrocatalyst, 2.0 mg of sample (0.85 mg /cm^2), 97µl ethanol, and 3µl Nafion were sonicated for 40 minutes, and then 0.003 ml of electrocatalyst ink was plunged on a glassy carbon electrode (GCE = working electrode) by micropipette. Pt wire and Hg/HgO were chosen as auxiliary and reference electrode correspondingly. The selected voltage window for electrocatalytic response through cyclic voltammetry (CV) and stability testing for 3600 seconds via chronoamperometry at a fixed potential of 0.69V was -0.1- 0.7 V (vs Hg/HgO). Moreover, the frequency range of 1 - $1x10^5$ Hz was picked to find out system resistance at amplitude of 0.005 V.

3.0. Results and Discussion

NiNH_2BDC MOF/1,2,5 wt % rGO hybrids were systematically evaluated through XPS, FTIR, XRD, SEM, Cyclic voltammetry , Tafel slope, Electrochemical impedance spectroscopy, EASA, mass activity, roughness factor, and Chronoamperometry.

In the FTIR spectrum of fabricated samples (Figure 2) the COO^{-1} group symmetric and asymmetric stretching vibrations generate resilient adsorption bands at the position of 1568 and 1374 cm^{-1} and the gap between these two bands designates the connection of the COO^{-1} group of the linker with nickel-metal through the bidentate mode of linking. The band at 1655 cm^{-1} besides 1250 cm^{-1} indicates the N-C group stretching mode of vibration as well as divulges the coordinated DMF group manifestation while NH_2 group stretching and bending vibrations bands appear at 3309 and 1684 cm^{-1}, respectively [56-59]. The region between 3300 and 3000 cm^{-1} was occupied by asymmetric & symmetric vibration bands of the H-N group [60]. C-H peak appears at 754 cm^{-1} while the evident peak at 587cm^{-1} approves the presence of nickel and its coordination with the COOH group oxygen [61, 62].

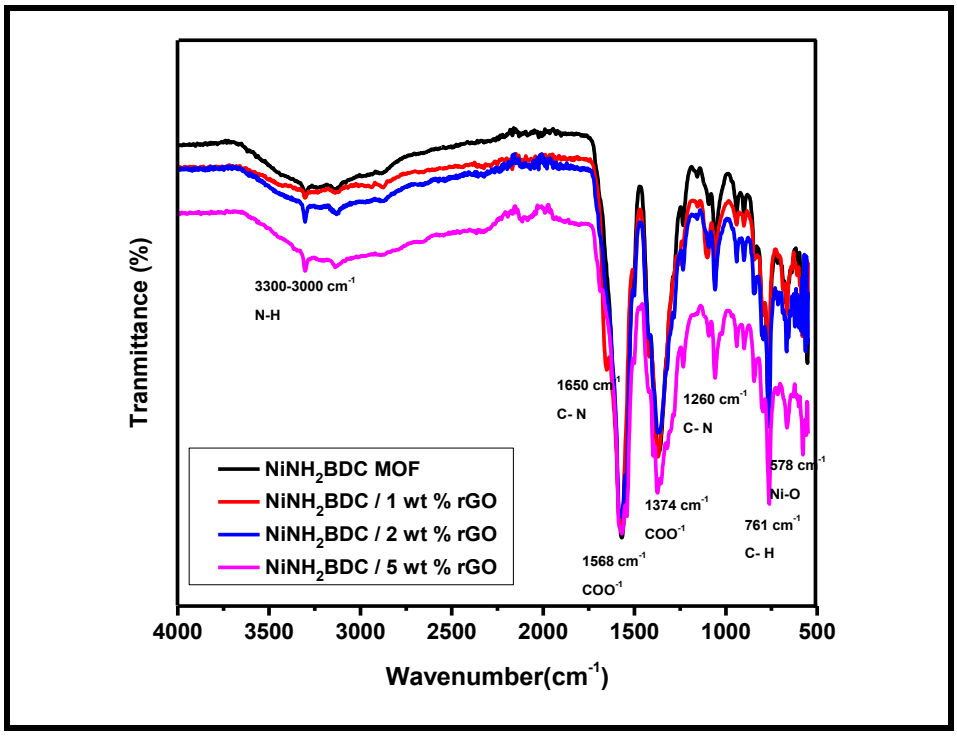

Figure 2. Fourier transformed infrared spectrum of $NiNH_2BDC$ MOF/1, 2, 5 wt % reduced graphitic carbon hybrids.

In the reported samples XRD pattern (Figure 3), less significant peaks within 2θ range of 42°-52° corresponds to the Ni NH_2BDC MOF distinctive peaks, while less intense peaks at 15°, 25°, 35°, 38°, 40°, and 61° ensure the development of Ni $(OH)_2$ during the reaction accompanied with DMF peak at 2θ, 7.5° and attributed to restricted hydrogen bonding leading to swelling effect and establishment of MOF pores (JCPDS. No:02-1216) [61, 63]. The rGO characteristics peaks are positioned at 17° and 23° and the gradual incline in peaks intensity from MOF to $NiNH_2BDC$/5 wt % rGO composite reflects the successful inclusion of rGO and composites synthesis [64, 65].

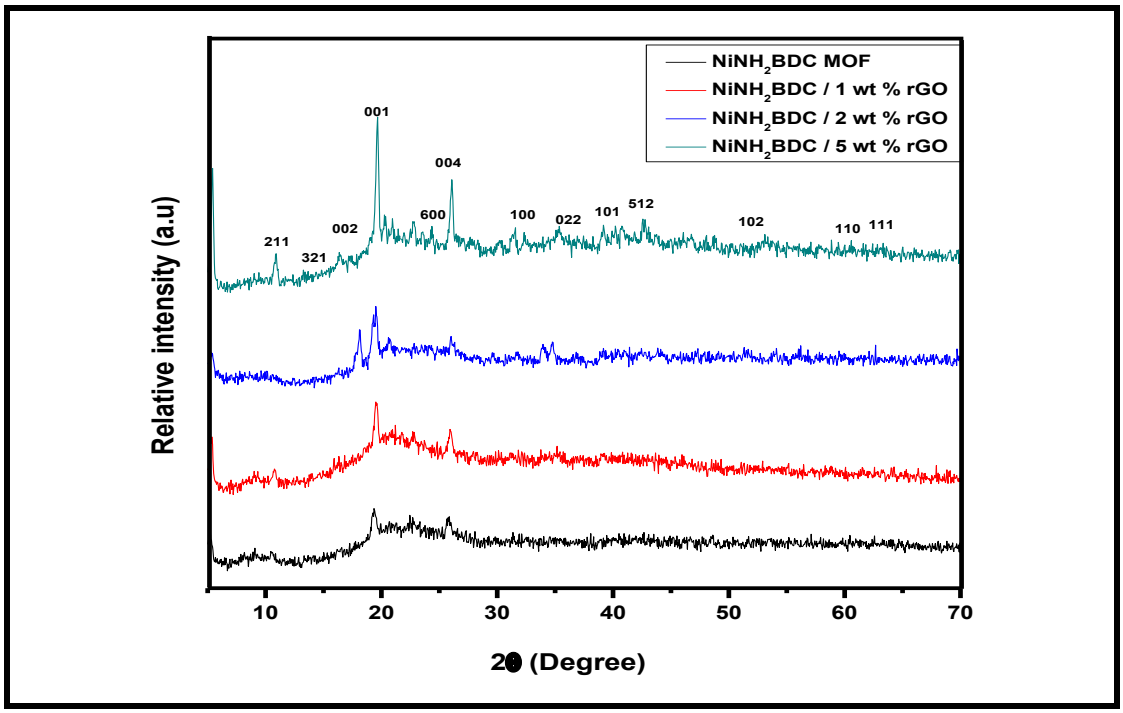

Figure 3. X-ray diffraction pattern of $NiNH_2BDC$ MOF/1, 2, 5 wt % reduced graphitic carbon hybrids.

The particle size, crystalline shape, and morphology appraised at different magnifications via SEM study display the presence of irregular shape particles (Figure 4a – 4h. Reduced graphene oxide sheets working as a MOF support are manifested in SEM images and they not only controls the size of MOF nanoparticles but also helps in a MOF NPs fine dispersal on its panes and prevents agglomeration [61, 66].

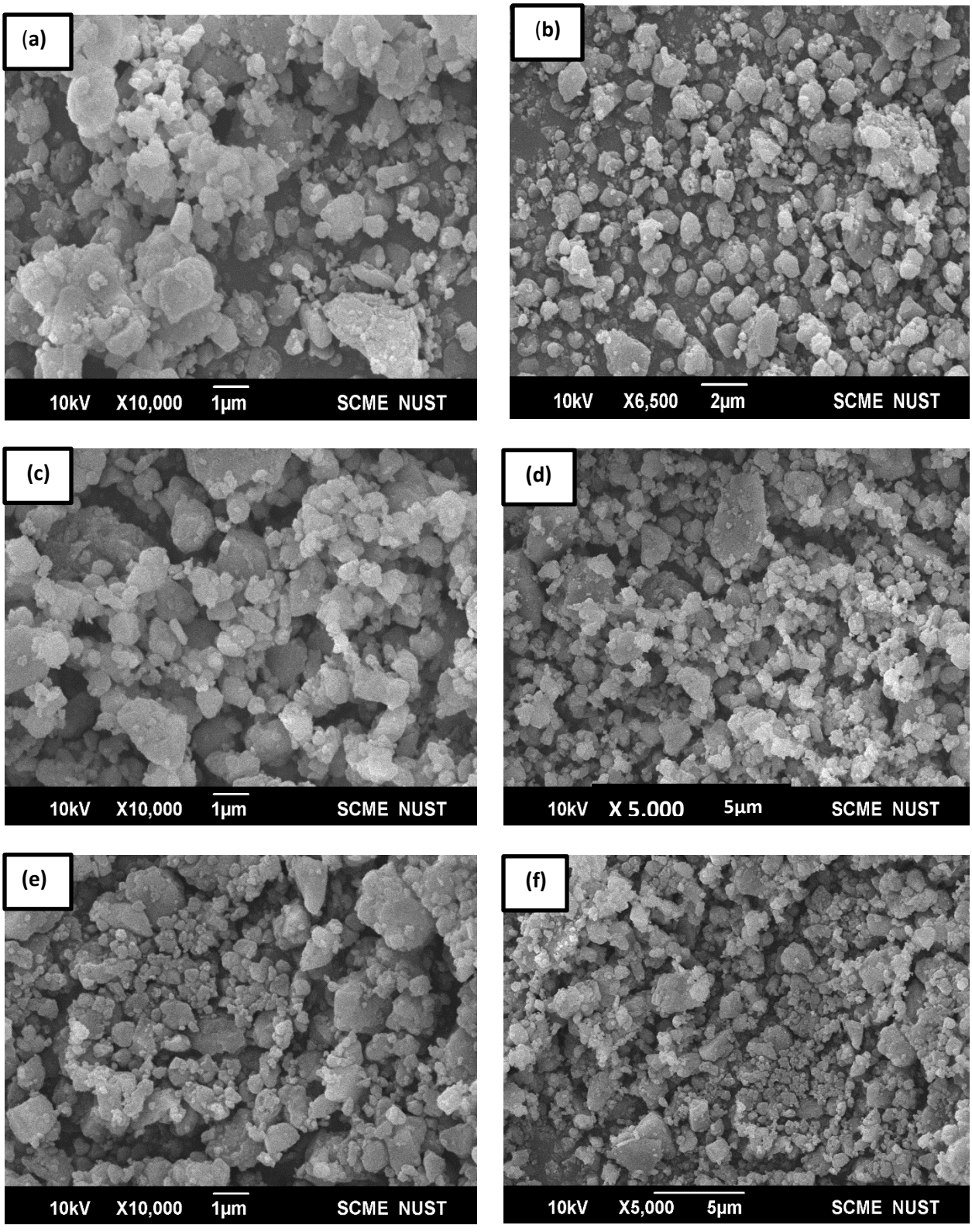
(a)
10kV X10,000 1µm SCME NUST
(b)
10kV X6,500 2µm SCME NUST
(c)
10kV X10,000 1µm SCME NUST
(d)
10kV X 5.000 5µm SCME NUST
(e)
10kV X10,000 1µm SCME NUST
(f)
10kV X5,000 5µm SCME NUST

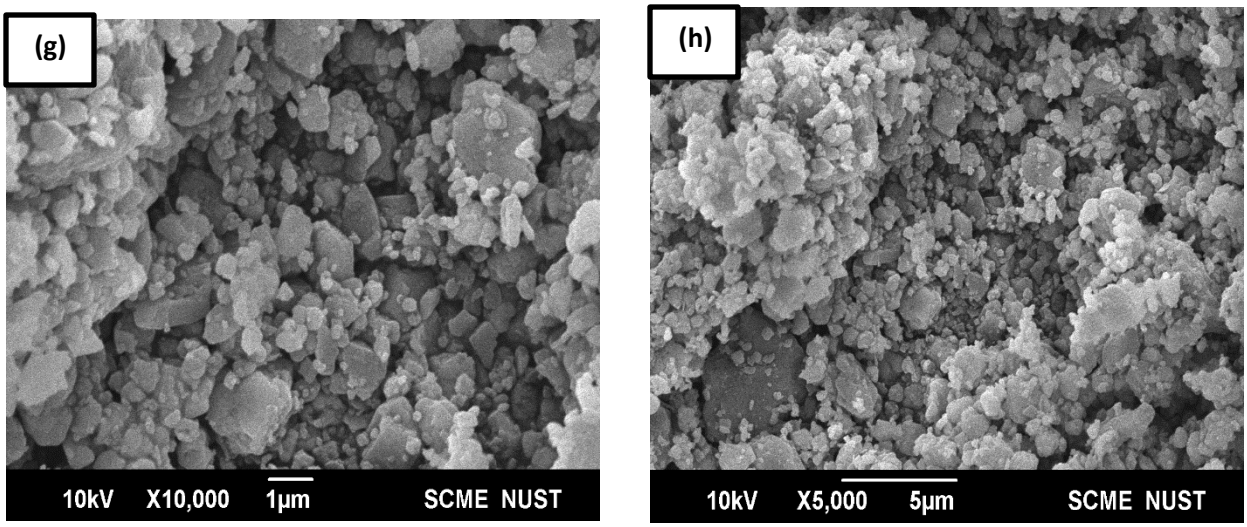

Figure 4. Scanning electron microscopy images of $NiNH_2BDC$ MOF (4a,4b), 1wt % rGO composite (4c,4d), 2 wt % rGO composite (4e,4f), and 5 wt % rGO composite (4g,4h) at different magnifications.

The information about elemental composition, binding energy, and metal oxidation state was obtained by XPS (Figure 5). The C 1s spectrum comprises 3 peaks at B.E (binding energy) value of 284, 286, and 288 eV stipulate the existence of C-C, C-O, and C=O groups, respectively while oxygen spectra deconvolution in 3 peaks with binding energy value of 530, 531, and 532 eV specifies the existence of M-O, C=O, and C-O. Fragmentation of nitrogen XPS spectra into two peaks of 402 and 403 eV represent the presence of the amine and pyrrolic nitrogen, respectively [67]. In nickel spectrum the presence of Ni^{+2}/Ni^{+3} was verified by the peaks in the range of 853-875 eV. The peaks at 871.8 eV for Ni $2p_{1/2}$ and 853.1 eV for Ni $2p_{3/2}$ indicates the spin-orbital coupling of Ni (+2) while peaks positioned at binding energy value of 874.73 eV (Ni $2p_{1/2}$) and 856.80 eV (Ni $2p_{3/2}$) are due to spin-orbital coupling of Ni (+3). The energy difference of 17.6 eV not only confirms the existence of Ni^{+2}/Ni^{+3} but also supports the nickel hydroxide manifestation [66, 68-73].

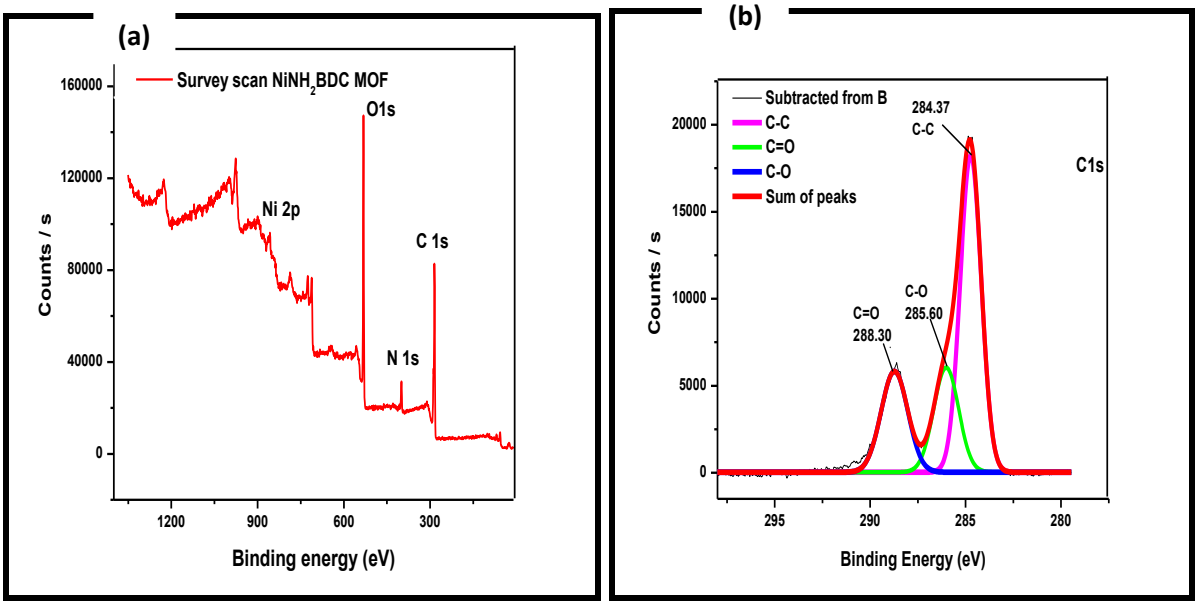
(a)
Survey scan NiNH2BDC MOF
O1s
Ni 2p
C 1s
N 1s
Counts / s
Binding energy (eV)
(b)
Subtracted from B
C-C
C=O
C-O
Sum of peaks
284.37
C-C
C1s
C-O
285.60
C=O
288.30
Counts / s
Binding Energy (eV)
(c)
Subtracted from B
C=O
C-O
M-O
PeakSum
O1s
531.89
C=O
532.35
C-O
530.15
M-O
Counts / s
Binding Energy (eV)
(d)
Subtracted from B
Pyrolic nitrogen
C-NH2
Baseline
Sum of peaks
N1s
400.02
C-NH2
398.82
Pyrolic nitrogen
Counts / s
Binding Energy (eV)

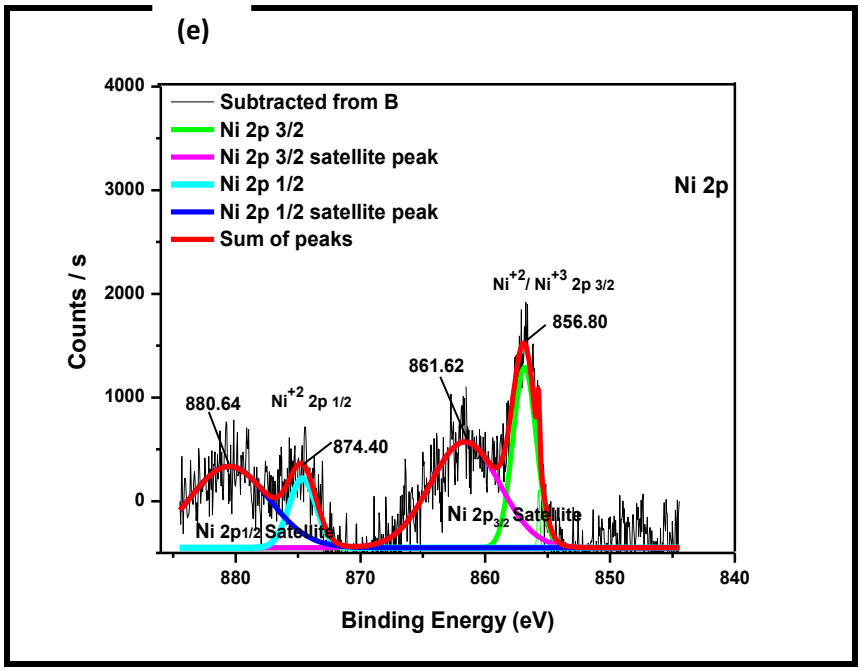

Figure 5. X-ray photoelectron spectra of $NiNH_2BDC$ (a) Survey scan (b) Carbon (c) Oxygen (d) Nitrogen, and (e) Nickel.

Raman spectrum obtained after interaction and scattering of electromagnetic radiation with matter gives an idea about crystalline and the defects rich nature of material [74-78]. Raman spectra of $NiNH_2BDC$ MOF rGO hybrids have been presented in Figure 6. In the selected range of analysis (4000-500 cm^{-1}) the G and D band appears due to graphitic carbon vibrations and carbon defects, respectively. The calculated I_d /I_g value is in following order; $NiNH_2BDC$ (0.95) < 1 wt % rGO composite (0.98) < 2 wt % rGO composite (1.003) < 5 wt % rGO composite (1.008). The (a) amplified I_d/I_g ratio in 5 wt % rGO composite due to rearrangements and structural defects promote the extensive π bonding and electron transfer from donor towards acceptor sites, and (b) ~5 and ~65-time shifting of G and D bands results in the smooth charge transfer process. Both of these factors attributed to enhanced catalytic activity of 5 wt %reduced graphitic carbon (rGO) hybrid than parent MOF [79].

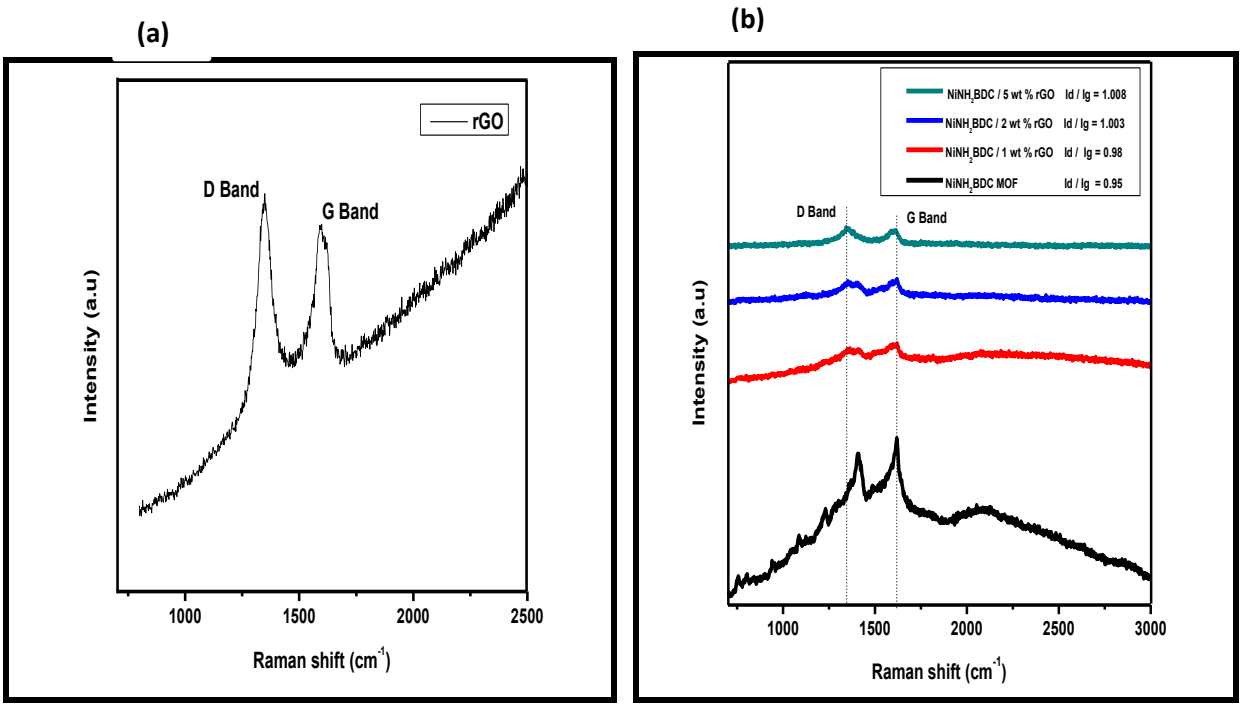

Figure 6. Raman spectra of (a) rGO (b) $NiNH_2BDC$ MOF/1, 2, 5 wt % reduced graphitic carbon hybrids.

3.1. Electrochemical Testing of $NiNH_2BDC$ MOF/1, 2, 5 wt % Reduced Graphitic Carbon Hybrids for MOR

1-3 mg of electrocatalyst was mounted on GCE to evaluate the optimized catalyst amount. The gradual increase in current density with respect to catalyst amount was due to easy access to abundant and exposed electroactive sites and after that decline in current density is due to; (i) restricted utilization of bottom layered material due to upper thick layer (ii) inferior charge transfer process, and (iii) active sites blockage by reaction intermediates (Figure 7a) [80-83]. Likewise, during methanol concentration optimization (1-5 M), the 3 M concentration with the maximum delivered current was found to be the optimum amount. At low content of CH_3OH, the boosted current response is owing to excess of available OH^- ions owing to diffusion-controlled methanol transport process while at high CH_3OH concentration, excess of methanol limit the OH^- adsorption,

and reaction intermediates block the active sites and consequently depress the catalytic activity, Figure 7b [84-86].

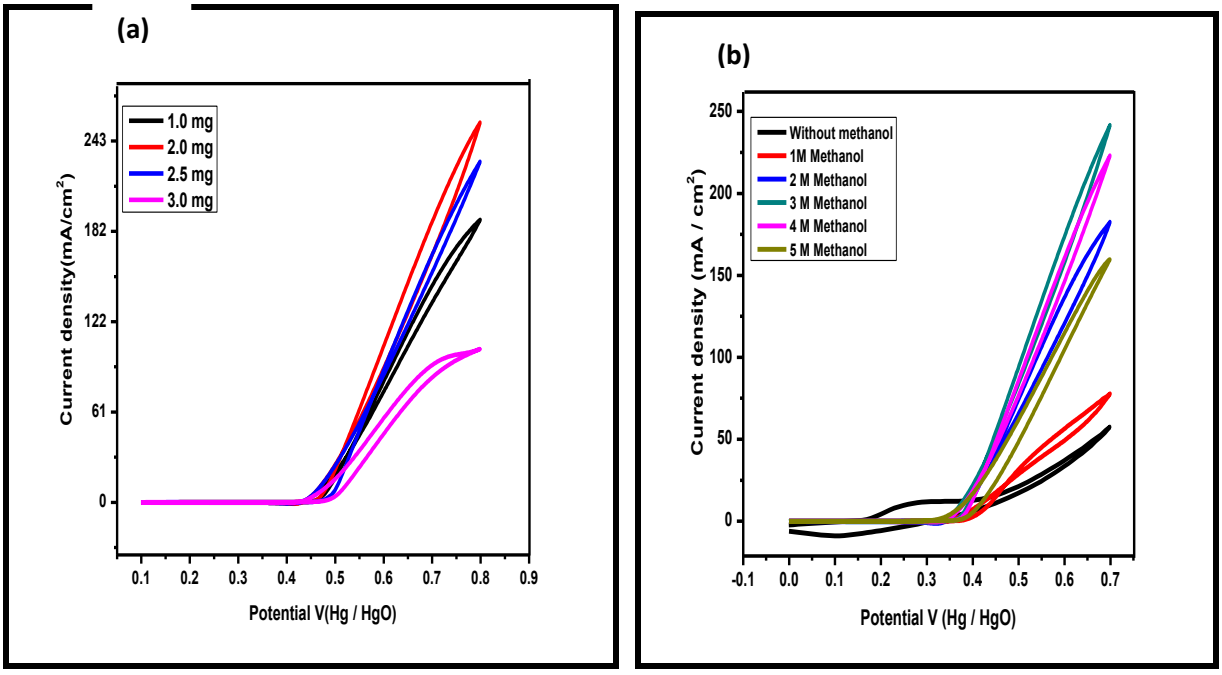

Figure 7. (a) Influence of electrocatalyst deposited quantity, and (b) CH_3OH molarity on the current density response of $NiNH_2BDC$ MOF/1, 2, 5 wt % reduced graphitic carbon hybrids during the optimization process.

The electrocatalytic response of all samples in the presence and absence of CH_3OH is compared and analyzed at 50 mV/ sec in Figure 8a, 8b. Without methanol, the 5.76 mA/cm^2 current density is produced while current density response of $NiNH_2BDC$ MOF/1-5 wt % reduced graphitic carbon hybrids is 181.01 ($NiNH_2BDC$) < 186.86 (1 wt % rGO) < 218.94 (2 wt % rGO)< ,and 267.77 (5 wt % rGO). Among all the analyzed composites the prime reason for the extraordinary current density of $NiNH_2BDC$/5 wt% rGO composite is; (a) synergistic effect between MOF and rGO (b) enhanced surface area, greater stability, and excellent conductivity due to sheet-like morphology of rGO. However, excessive rGO amount in $NiNH_2BDC$/6 wt % rGO composite results in (i) rGO sheets restacking due to pi-pi interaction and choked active sites (ii) inhibited methanol diffusion,

and (iii) firmly attached reaction intermediate (CO) limiting OH^- ions adsorption on electrode surface [24, 64, 87-89].

The cyclic voltametric investigations were executed at the scanning speed of 2, 5, 10, 25, and 50 mV/sec by selecting the voltage window of -0.1- 0.7 to recognize the influence of scanning speed on the current density of the tested samples. At the highest scanning speed, the easy and maximum approach of electroactive species towards the electrode surface leads to maximum current density Figure 8 b-f [90, 91].

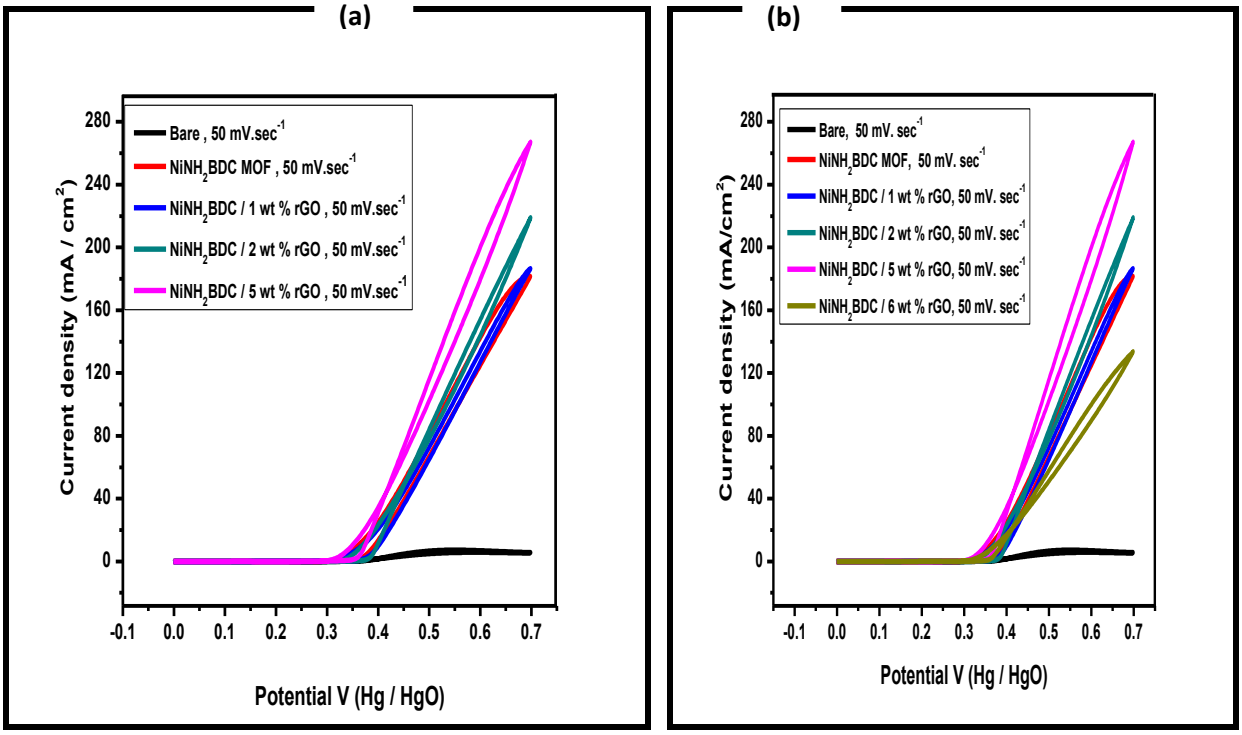

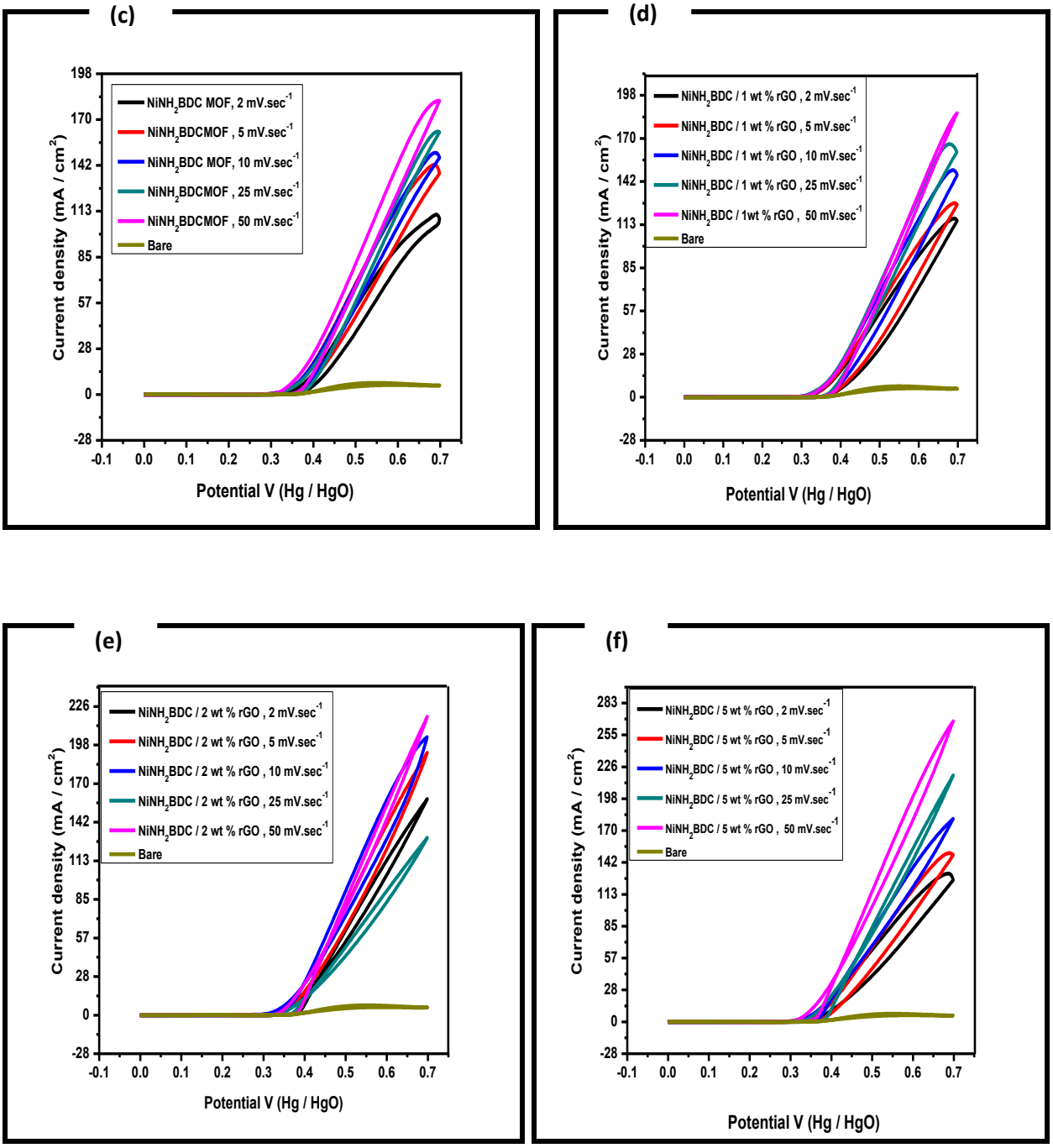

Figure 8. Cyclic voltamogram of (a) $NiNH_2BDC$ MOF/1-5 wt % reduced graphitic carbon hybrids at 50 mV/ sec (b) $NiNH_2BDC$ MOF/1-6 wt % reduced graphitic carbon hybrids at 50 mV/ sec (c) $NiNH_2BDC$ MOF (d) $NiNH_2BDC$/1 wt % reduced graphitic carbon hybrids (e)

NiNH$_2$BDC/2 wt % reduced graphitic carbon hybrids, and (f) NiNH$_2$BDC/5 wt % reduced graphitic carbon hybrids in 3 M CH$_3$OH /1 M NaOH solution at scanning speed 2–50 mV/sec. To get information about the diffusion-controlled process, a straight line obtained by directly relating the peak current density with (scan rate) $^{1/2}$, provides a slop that is equivalent to diffusion co-efficient (Figure 9). Furthermore, the diffusion co-efficient (D) is calculated by inserting value of the α (charge transfer coefficient) in the Randles Sevcik equation [92].

$$Ip = (2.99 \times 10^5)\, n\, (\alpha\, n_\alpha)^{1/2} A\, C\, D^{1/2}\, \nu^{1/2}$$

For non-reversible oxidation process, the calculated D (diffusion coefficient) value are; 13.2 x 10^{-5} cm^2.s^{-1} for NiNH$_2$BDC MOF, 16.1 x 10^{-5} cm^2.s^{-1} for 1wt % rGO composite, 21.8 x 10^{-5} cm^2 .s^{-1} for 2wt% rGO composite, and 31.8 x 10^{-5} cm^2.s^{-1} for 5wt% rGO composite, respectively (Table 1). R^2 value ≈ 1 and absolute value of diffusion co-efficient for NiNH$_2$BDC 5wt % rGO composite prove it to be active MOR catalyst [93].

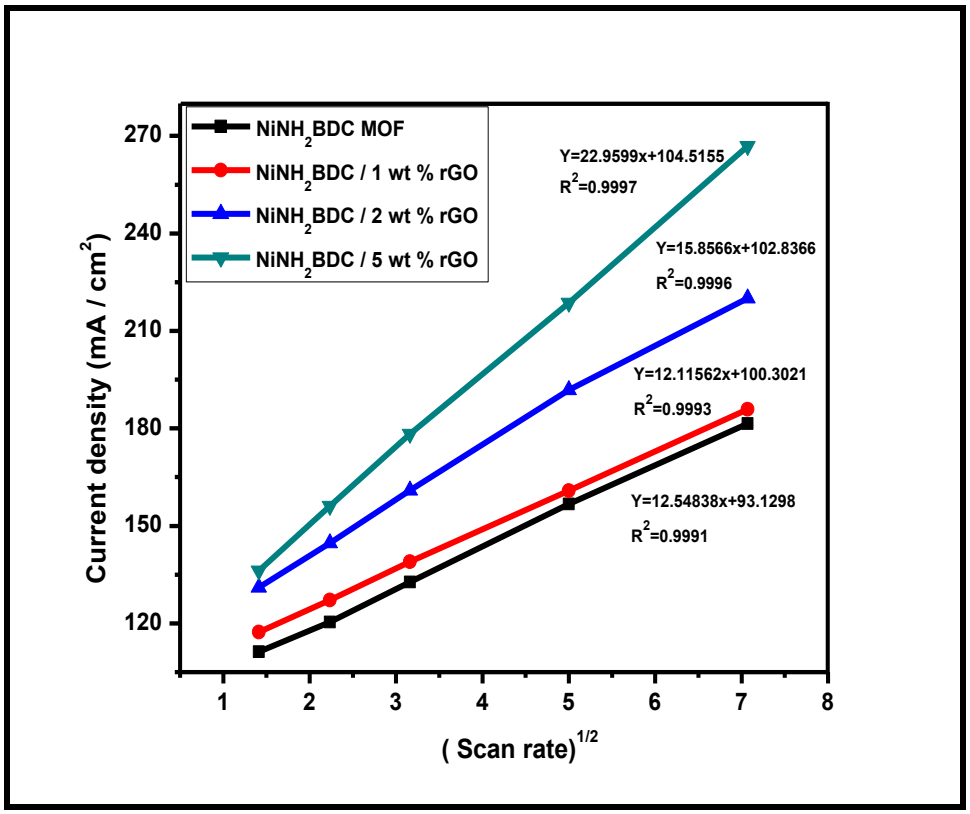

Figure 9. A graphical representation of the direct relationship of peak current density (j) vs under root of scan rate (ν) in 3M CH_3OH/1 M NaOH solution.

Table 1. The comparative statement of the magnitude of diffusion co-efficient and R^2 of $NiNH_2BDC$ MOF/1, 2, 5 wt % reduced graphitic carbon hybrids at 50 mV/sec.

Electrocatalyst	**R^2**	**Diffusion Coefficient**
$NiNH_2BDC$ MOF	0.9991	13.2 x 10^{-5} $cm^2.s^{-1}$
$NiNH_2BDC$ / 1wt % rGO	0.9993	16.1 x 10^{-5} $cm^2.s^{-1}$
$NiNH_2BDC$ / 2wt % rGO	0.9996	21.8 x 10^{-5} $cm^2.s^{-1}$
$NiNH_2BDC$ / 5wt % rGO	0.9997	31.8 x 10^{-5} $cm^2.s^{-1}$

The EIS (Electrochemical impedance spectroscopy), an important parameter tend to explore the kinetics and reaction mechanism. The EIS evaluation was accomplished in 3 electrode systems within selected frequency domain of 1-1x10^5 Hz in an alkaline solution. Figure 10a and 10b illustrate the Nyquist plot of the bare electrode and $NiNH_2BDC$ MOF/rGO composites. A depressed semicircle of $NiNH_2BDC$/5 wt % rGO hybrid illustrates the lowermost resistance (highest conductivity) than other counterparts due to homogenous scattering of MOF NPs on rGO surface having high surface area, exposed electroactive sites with maximum OH^- adsorption, facile CO oxidation, smooth charge and mass transfer, and accelerated CH_3OH oxidation process [94]. Besides, modification of interfacial structure as a result of rGO inclusion is also an important kinetic controlling factor [95-97]. The extracted EIS data obtained after fitting a suitable circuit represent the minimum contact resistance, electrolyte resistance, and substrate inherent resistance

with consequent excellent conductivity and electrocatalytic activity of $NiNH_2BDC$/5 wt % rGO (Table 2) [98, 99].

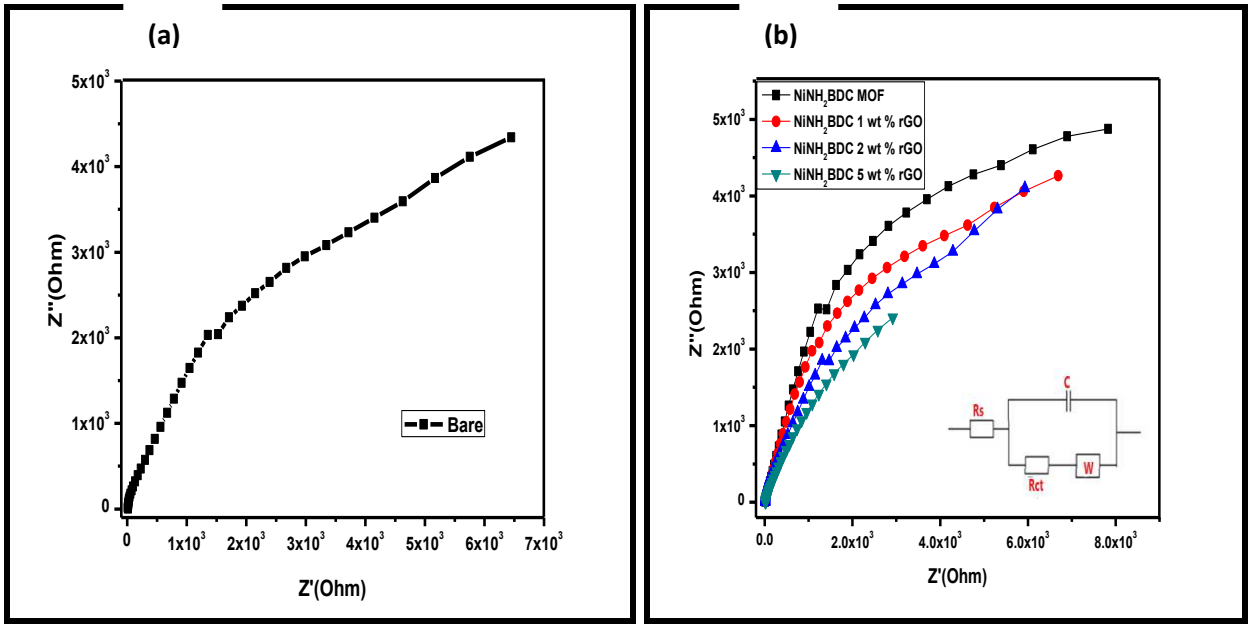

Figure 10. Nyquist plot (a) Bare and (b) $NiNH_2BDC$ MOF/1, 2, 5 wt % reduced graphitic carbon hybrids in 3 M CH_3OH/1 M NaOH solution at oxidation potential 0.699 V.

Table 2. Capacitance (C), Warburg diffusion co-efficient (W), charge transfer resistance (Rct), and resistance of solution (Rs) of $NiNH_2BDC$ MOF/1, 2, 5 wt % reduced graphitic carbon hybrids plucked from EIS information of MOR process

Catalyst	**Rs (Ω)**	**Rct (Ω)**	**Capacitance (F)**	**Warburg Diffusion Co-efficient (W)**
Bare	18.84	86.24	492.1 $x10^{-9}$	33.89 $x10^{-6}$
$NiNH_2BDC$ MOF	14.24	67.13	538.5$x10^{-9}$	39.97 $x10^{-6}$
$NiNH_2BDC$ / 1 wt % rGO	14.10	63.10	540.8$x10^{-9}$	40.09 $x10^{-6}$

$NiNH_2BDC$ / 2 wt % rGO	13.33	58.35	$548.8x10^{-9}$	$43.16\ x10^{-6}$
$NiNH_2BDC$ / 5 wt % rGO	13.26	35.50	$1.072x10^{-6}$	$92.33\ x10^{-6}$

Tafel plot is another important parameter utilized for evaluation of methanol oxidation activity, reaction mechanism, and kinetics of catalytic process by co-relating ln current density (ln j) with overpotential (η) (Figure 11). Over potential is the required potential greater than the requisite potential for a reaction to ensue. The kinetic behavior of as-synthesized samples is determined by given below Tafel equation [100].

$$\eta = A + b \log j$$

At low overpotential (0.388 V), the $NiNH_2BDC$ MOF/1, 2, 5 wt % rGO composites calculated Tafel slope values are in order of; 62.0 (pure MOF) > 61.6 (1wt % rGO) > 59.6 (2 wt % rGO) > 57.3 mV/dec (5 wt % rGO), respectively. Moreover, at comparatively greater overpotential (0.410 V), the Tafel slope follow the sequence of; 65.4 (pure MOF) > 65.1(1wt % rGO) > 63.0 (2wt % rGO) > 60.8 mV/dec (5 wt % rGO) (Table 3). Two different informations are obtained by calculating the Tafel slope at low and high overpotential region as (a) Hydrogen removal (dehydrogenation) from CH_3OH is the rate controlling step in low potential region while (b) CO exclusion during oxidation process occur in the escalated potential domain. The $NiNH_2BDC$/5 wt % rGO composite lowermost Tafel slope value (57.3 mV/dec) reflects the fast removal of hydrogen from CH_3OH during oxidation process [101-105].

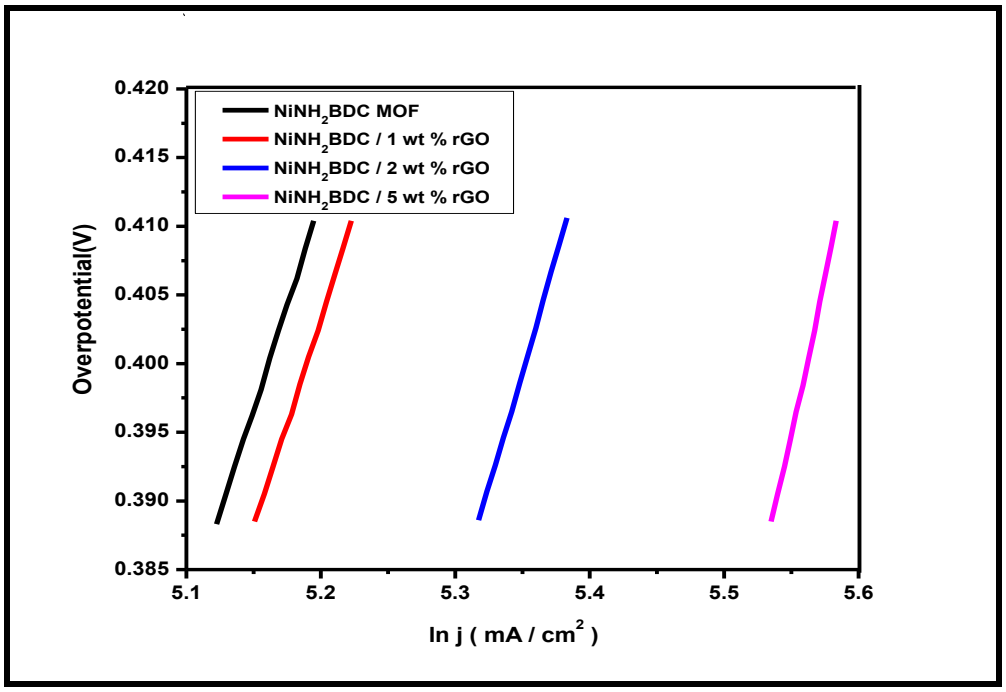

Figure 11. Tafel plot (η vs ln j) of $NiNH_2BDC$ MOF/1, 2, 5 wt % reduced graphitic carbon hybrids in 3 M CH_3OH/1 M NaOH solution.

Table 3. The Tafel slope values of $NiNH_2BDC$ MOF/1, 2, 5 wt % reduced graphitic carbon hybrids at high and low overpotential.

Electrocatalyst	**Tafel slope ($mV.dec^{-1}$)** **η = 0.388 V**	**Tafel slope ($mV.dec^{-1}$)** **η = 0.410 V**
$NiNH_2BDC$ MOF	62.0	65.4
$NiNH_2BDC$ / 1wt % rGO	61.6	65.1
$NiNH_2BDC$ / 2wt % rGO	59.6	63.1
$NiNH_2BDC$ / 5wt % rGO	57.3	60.8

The utmost requirement for practical application of electrocatalyst is its long term stability under experimental conditions. A chronoamperometry (*i*/*t*) experiment is conducted in N_2 saturated alkali solution at peak potential 0.69 V vs Hg/HgO in three electrodes set up for 60 minutes. The graphical response of the oxidation process can be elaborated as (i) initial maximum j (current density) is due to strong binding of catalyst at electrode surface, minimum gas bubbles, and large available active sites. (ii) The rapid decline in current density after a short period is associated with (a) extreme gas release and reaction intermediates formation which block the electroactive sites, and(b) material detachment due to excessive bubbling (iii) finally, a steady-state is achieved which persists for 3600 seconds due to the reaction intermediates passive adsorption [106-109]. According to chronoamperometry graph, the stability retained by $NiNH_2BDC$/5 wt % rGO composite is 60.6 % while the stability retained by remaining samples is; $NiNH_2BDC$/2 wt % rGO 59.3 %, $NiNH_2BDC$/1 wt % rGO 59.0 %, and $NiNH_2BDC$ MOF 57.3 %, respectively (Figure 12 a, b). The minimum loss in current density of $NiNH_2BDC$/5 wt % rGO composite attributed to (a) large specific surface area provided by 2D rGO sheets (b) tolerance towards poisonous reaction intermediates (c) fine scattering of small size MOF nanoparticles on rGO surface, and trivial charge transfer resistance [104].

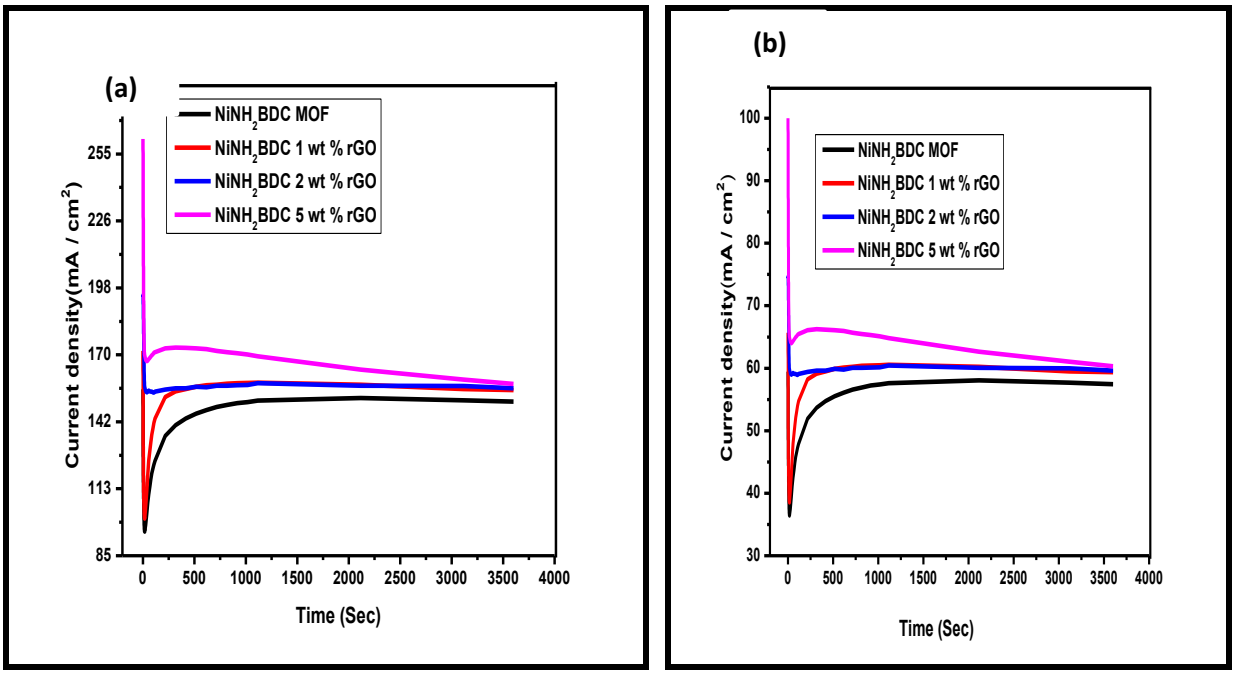

Figure 12. (a) Stability trend of $NiNH_2BDC$ MOF/1, 2, 5 wt% reduced graphitic carbon hybrids and (b) % stability retained by samples in 3M CH_3OH/1 M NaOH solutions at oxidation potential of 0.69 V vs Hg / HgO for 3600 seconds.

The recommended mechanism for the CH_3OH oxidation process is as under [110, 111].

$$Ni^{o} + 2OH^{-} \longrightarrow Ni^{+2}(OH)_2 \quad (1)$$

$$Ni^{+2}(OH)_2 \longrightarrow Ni^{+3}(OH)_2 + e^{-} \quad (2)$$

$$Ni^{+3}(OH)_2 + OH^{-} \longrightarrow Ni^{+3}(OH)_3 \quad (3)$$

$$Ni^{+3}(OH)_3 \longrightarrow NiOOH + H_2O \quad (4)$$

$$NiOOH + CH_3OH_{(ads)} \longrightarrow Ni^{+2}(OH)_2 + (CH_2O)_{ads} \quad (5)$$

$$NiOOH + (CH_2O)_{(ads)} \longrightarrow Ni^{+2}(OH)_2 + (CHO)_{ads} \quad (6)$$

$$NiOOH + (CHO)_{(ads)} \longrightarrow Ni^{+2}(OH)_2 + (CO)_{ads} \quad (7)$$

$$NiOOH + (CHO)_{(ads)} \longrightarrow Ni^{+2}(OH)_2 + CO_2 \quad (8)$$

In the case of a Nickel-based system, NiO smoothened the CO oxidation by providing required oxygen while the NiOOH group promotes the MOR by Ni^{+2} / Ni^{+3} oxidation/reduction process where +2 to +3 oxidation further promote CO oxidation [112, 113].

The mass activity of all electrocatalysts is determined from the ratio of the current density vs deposited mass

$$\text{Mass activity} = J / m$$

The mass activity (M.A) of tested samples at an overpotential of 0.331 V is as under; $NiNH_2BDC$ MOF 113.8 mA/mg < $NiNH_2BDC$/1 wt % rGO composite 120.4 mA/mg < $NiNH_2BDC$ /2 wt % rGO composite 133.8 mA/mg < and $NiNH_2BDC$ / 5 wt % rGO composite 168.7 mA/mg.

To calculate the electrocatalytic activity of as-synthesized samples, EASA (Electrochemically active surface area) is determined by dividing Cdl (double-layer capacitance) with Cs (specific capacitance). Specific capacitance is a constant factor for each specific system while double-layer capacitance is determined through multiple CV scans or EIS in the non-faradic region. The estimated EASA of $NiNH_2BDC$ MOF/1, 2, 5 wt % reduced graphitic carbon hybrids at voltage 0.19 was observed to be ; 7.6 (pure MOF) < 9.1 (1 wt % rGO) < 14.4 (2 wt % rGO) < 15.7(5 wt % rGO), correspondingly. The comparatively heightened catalytically active surface area of $NiNH_2BDC$/ 5 wt % rGO composite proves the superb electrocatalytic performance of material for MOR (Supplementary information Figure 1). The given data also authenticate the CV, EIS, and Tafel results.

Moreover, the EASA is divided with geometrical area of electrode to calculate the R.F (roughness factor). It is a unit less factor, as it is a ratio.

$$\text{R.F} = \text{EASA / Electrode geometrical area}$$

The heightened roughness factor reflects the excellent catalytic performance of material due to direct relationship between EASA and R.F. Roughness factor of $NiNH_2BDC$ MOF/1-5 wt % reduced graphitic carbon hybrids was found in the following order; 107, 128, 204, and 222 respectively (Table 4 and Figure 13) [114].

Table 4. EASA, Mass activity, and Roughness factor comparison of $NiNH_2BDC$ MOF/1, 2, 5 wt % reduced graphitic carbon hybrids.

Catalyst	EASA (cm^2)	Mass activity (mA / mg)	Roughness Factor
$NiNH_2BDC$ MOF	7.6	113.8	107
$NiNH_2BDC$ / 1wt % rGO	9.1	120.3	128
$NiNH_2BDC$ / 2wt % rGO	14.1	133.8	204
$NiNH_2BDC$ / 5wt % rGO	15.7	168.7	222

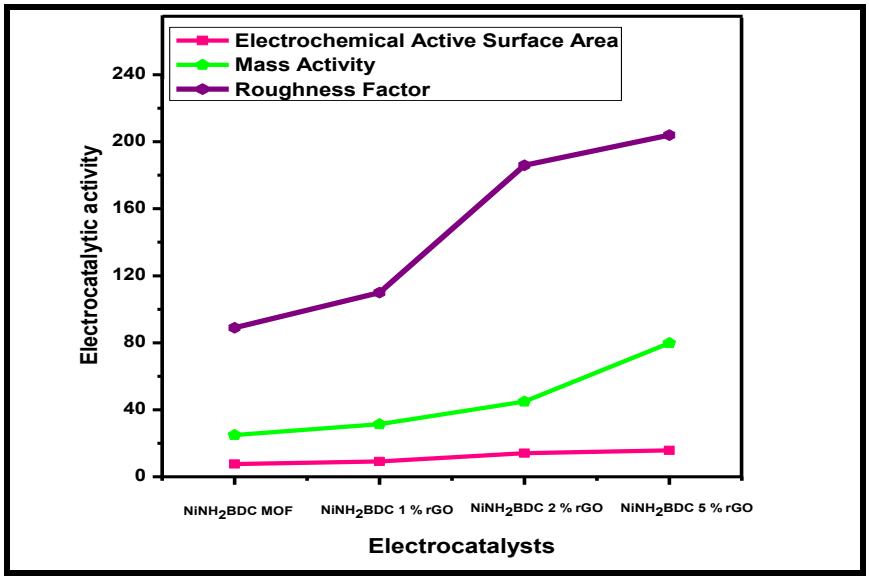

Figure 13. Comparison of EASA, Mass activity, and Roughness factor of $NiNH_2BDC$ MOF / 1, 2, 5 wt % reduced graphitic carbon hybrids.

The comparative statement of the electrocatalytic response of tested materials with already reported materials is provided in Table 5 given below.

Table 5. The electrocatalytic activity of synthesized samples in comparison with reported materials

Electrocatalytic materials	**Molarity of Methanol solution (M)**	**Scan rate ($mV.\ s^{-1}$)**	**Oxidation potential (V) vs RHE**	**Anodic current density ($mA.cm^{-2}$)**	**Resistance (Ω)**	**Ref**
Pt / rGO	3M	50	1.72	32	-	[115]
NiO-MOF/rGO	3M	50	1.83	276	22.8	[23]
Cu BTC / 5 wt % rGO	3M	50	1.84	120	20.53	[22]
Ni Cr LDH	3M	50	1.63 V	7.02	-	[116]
$NiNH_2BDC$ MOF	3M	50	1.614 V	180.0	14.24	This work
$NiNH_2BDC$ / 1 wt % rGO	3M	50	1.614 V	186.8	14.10	This work

$NiNH_2BDC$ / 2 wt % rGO	3M	50	1.614 V	218.94	13.33	This work
$NiNH_2BDC$ / 5 wt % rGO	3M	50	1.614 V	267.77	13.26	This work

4.0. Conclusions

The $NiNH_2BDC$ MOF/1-5 wt % reduced graphitic carbon hybrids ($NiNH_2BDC$/rGO) fabricated by sonication assisted solvothermal approach were studied for CH_3OH oxidation process under alkaline condition. The $NiNH_2BDC$ MOF/5 wt % rGO composite by possessing auspicious current of 267.7 $mA.cm^{-2}$ at voltage 0.69, Tafel slope of 60.8 $mV.dec^{-1}$, resistance of 13.26 Ω, EASA 15.7 cm^2, mass activity 168.7 mA/mg and roughness factor 222 in 3 M CH_3OH/1 M NaOH solution displays better activity a s compared to state-of-the-art platinum-based materials and prove to be a proficient substitute of costly materials exploited for MOR in direct CH_3OH fuel cell.

Acknowledgments

The author would like to appreciate the contribution of School of Natural Sciences (SNS), the School of Chemical and Material Engineering (SCME), and US-Pakistan Center for Advanced Studies in Energy (USPCAS-E) at NUST in terms of all lab amenities.

References

[1] S. Chu and A. Majumdar, Opportunities and challenges for a sustainable energy future. nature. **488**, 294-303 (2012). https://doi.org/10.1038/nature11475

[2] A. L. M. Reddy, S. R. Gowda, M. M. Shaijumon, and P. M. Ajayan, Hybrid nanostructures for energy storage applications. Adv.Mater.**24**,5045-5064(2012). https://doi.org/10.1002/adma.201104502.

[3] H. Wang and H. Dai, Strongly coupled inorganic–nano-carbon hybrid materials for energy storage. Chem.Soc.Rev. **42**, 3088-3113 (2013). https://doi.org/10.1039/C2CS35307E.

[4] N. S. Choi, Z. Chen, S. A. Freunberger, X. Ji, Y. K. Sun, K. Amine, et al., Challenges facing lithium batteries and electrical double-layer capacitors. Angew.Chem. Int.Ed. **51**, 9994-10024 (2012). https://doi.org/10.1002/anie.201201429.

[5] B. C. Steele and A. Heinzel, Materials for fuel-cell technologies.Nature. 224-231(2011). https://doi.org/10.1142/9789814317665_0031

[6] C. Coutanceau, R. Koffi, J.-M. Léger, K. Marestin, R. Mercier, C. Nayoze, et al., Development of materials for mini DMFC working at room temperature for portable applications. J.power sources. **160**.334-339 (2006). https://doi.org/10.1016/j.jpowsour.2006.01.073.

[7] D. Borello, A. Calabriso, L. Cedola, L. Del Zotto, and S. G. Santori, Development of improved passive configurations of DMFC with reduced contact resistance. Energy Procedia. **61**. 7 (2014). https://doi.org/10.1016/j.egypro.2014.12.268.

[8] L. Wang, Z. Yuan, F. Wen, Y. Cheng, Y. Zhang, and G. Wang, A bipolar passive DMFC stack for portable applications. Energy. **144.** 587-593 (2018). https://doi.org/10.1016/j.energy.2017.12.039.

[9] R. Dillon, S. Srinivasan, A. Arico, and V. Antonucci, International activities in DMFC R&D: status of technologies and potential applications. J. Power Sources. **127**. 112-126 (2004). https://doi.org/10.1016/j.jpowsour.2003.09.032.

[10] N. K. Shrivastava, S. B. Thombre, and R. B. Chadge, Liquid feed passive direct methanol fuel cell: challenges and recent advances. Ionics. **22**. 1-23 (2016). https://doi.org/10.1007/s11581-015-1589-6.

[11] R. Chen and T. Zhao, "Mathematical modeling of a passive-feed DMFC with heat transfer effect. J. Power Sources. **152**. 122-130 (2005). https://doi.org/10.1016/j.jpowsour.2005.02.088.

[12] G. Gwak, K. Lee, S. Ferekh, S. Lee, and H. Ju, Analyzing the effects of fluctuating methanol feed concentration in active-type direct methanol fuel cell (DMFC) systems. Int. j. Hydrog. Energy. **40**. 5396-5407 (2015). https://doi.org/10.1016/j.ijhydene.2015.01.062.

[13] T. Zhao, R. Chen, W. Yang, and C. Xu, Small direct methanol fuel cells with passive supply of reactants. J. Power Sources. **191**. 185-202 (2009). https://doi.org/10.1016/j.jpowsour.2009.02.033.

[14] S. Hanif, N. Iqbal, X. Shi, T. Noor, G. Ali, and A. Kannan, NiCo-N-doped carbon nanotubes based cathode catalyst for alkaline membrane fuel cell. Renew. Energy. **154.** 508-516 (2020). https://doi.org/10.1016/j.renene.2020.03.060.

[15] S. A. M. Rizvi, N. Iqbal, M. D. Haider, T. Noor, R. Anwar, and S. Hanif, Synthesis and Characterization of Cu-MOF Derived Cu@ AC Electrocatalyst for Oxygen Reduction Reaction in PEMFC. Catal Letters. **150**. 1-11 (2019). https://doi.org/10.1007/s10562-019-03024-x.

[16] H. Hu, H. Cheng, J. Zhou, Q. Zhu, and Y. Yu, Hierarchical porous Fe2O3 assisted with graphene-like carbon as high-performance lithium battery anodes. Mater.Today Phys. **3**. 7-15 (2017). https://doi.org/10.1016/j.mtphys.2017.10.004.

[17] J. Shuai, J. Mao, S. Song, Q. Zhang, G. Chen, and Z. Ren, Recent progress and future challenges on thermoelectric Zintl material. Mater.Today Phys. **1**. 74-95 (2017). https://doi.org/10.1016/j.mtphys.2017.10.004.

[18] A. Hacquard, Improving and understanding direct methanol fuel cell (DMFC) performance. 2005.

[19] E. Reddington, A. Sapienza, B. Gurau, R. Viswanathan, S. Sarangapani, E. S. Smotkin, et al.,Combinatorial electrochemistry: a highly parallel, optical screening method for discovery of better electrocatalysts. Science. **280**. 1735-1737 (1998).http://doi.: 10.1126/science.280.5370.1735.

[20] Y. Lin, X. Cui, C. H. Yen, and C. M. Wai, PtRu/carbon nanotube nanocomposite synthesized in supercritical fluid: a novel electrocatalyst for direct methanol fuel cells. Langmuir. **21**. 11474-11479 (2005). https://doi.org/10.1021/la051272o.

[21] L. Cao, F. Scheiba, C. Roth, F. Schweiger, C. Cremers, U. Stimming, et al., Novel Nanocomposite Pt/RuO2· x H2O/Carbon Nanotube Catalysts for Direct Methanol Fuel Cells. Angew. Chem.Int.Ed.**45**.5315-5319(2006). https://doi.org/10.1002/anie.200601301.

[22] T. Noor, M. Ammad, N. Zaman, N. Iqbal, L. Yaqoob, and H. Nasir, A highly efficient and stable copper BTC metal organic framework derived electrocatalyst for oxidation of methanol in DMFC application. Catal Letters. **149.** 3312-3327 (2019). https://doi.org/10.1007/s10562-019-02904-6.

[23] T. Noor, N. Zaman, H. Nasir, N. Iqbal, and Z. Hussain, Electro catalytic study of NiO-MOF/rGO composites for methanol oxidation reaction. Electrochim. Act. **307**. 1-12 (2019). https://doi.org/10.1016/j.electacta.2019.03.116.

[24] L. Bai, Synthesis of PtRu/Ru heterostructure for efficient methanol electrooxidation: the roleofextraRu.Appl.Surf.Sci.**433.**279-284(2018). https://doi.org/10.1016/j.apsusc.2017.10.026.

[25] M. Watanabe and S. Motoo, Electrocatalysis by ad-atoms: Part II. Enhancement of the oxidation of methanol on platinum by ruthenium ad-atoms. J. Electroanal. Chem. **60**, 267-273 (1975). https://doi.org/10.1016/S0022-0728(75)80261-0.

[26] A. G. Vidales, L. Dam-Quang, A. Hong, and S. Omanovic,The influence of addition of iridium-oxide to nickel-molybdenum-oxide cathodes on the electrocatalytic activity towards hydrogen evolution in acidic medium and on the cathode deactivation resistance. Electrochim. Act. **302**. 198-206 (2019). https://doi.org/10.1016/j.electacta.2019.02.030.

[27] I. Kodintsev and S. Trasatti,Electrocatalysis of H2 evolution on RuO2+ IrO2 mixed oxide electrodes. Electrochim.act. **39.** 1803-1808 (1994). https://doi.org/10.1016/0013-4686(94)85168-9.

[28] W. Du, Y.-L. Bai, J. Xu, H. Zhao, L. Zhang, X. Li, et al.,Advanced metal-organic frameworks (MOFs) and their derived electrode materials for supercapacitors. J. Power Sources. **402**. 281-295 (2018). https://doi.org/10.1016/j.jpowsour.2018.09.023.

[29] T. Zhang, Y. Jin, Y. Shi, M. Li, J. Li, and C. Duan, Modulating photoelectronic performance of metal–organic frameworks for premium photocatalysis.Coord.Chem. Rev. **380.** 201-229 (2019). https://doi.org/10.1016/j.ccr.2018.10.001.

[30] T. Toyao, M. Saito, Y. Horiuchi, K. Mochizuki, M. Iwata, H. Higashimura, et al., Efficient hydrogen production and photocatalytic reduction of nitrobenzene over a visible-light-responsive metal–organic framework photocatalys. Catal. Sci.Technol. **3**. 2092-2097 (2013). https://doi.org/10.1039/C3CY00211J.

[31] S. Zhao, Y. Wang, J. Dong, C.-T. He, H. Yin, P. An, et al., Ultrathin metal–organic framework nanosheets for electrocatalytic oxygen evolution. Nat. Energy. **1**.1-10 (2016). https://doi.org/10.1038/nenergy.2016.184.

[32] T. Hickson, Identifying the top 20 per cent. Interview by Christian Martin, Nat. Mater. **11**. 6 (2011). https://doi.org/10.1038/nmat3208.

[33] M. H. Hassan, A. B. Soliman, W. A. Elmehelmey, A. A. Abugable, S. G. Karakalos, M. Elbahri, et al., A Ni-loaded, metal–organic framework–graphene composite as a precursor for in situ electrochemical deposition of a highly active and durable water oxidation nanocatalyst. Chem.Commun. **55**.31-34 (2019). https://doi.org/10.1039/C8CC07120A.

[34] E. Sarwar, T. Noor, N. Iqbal, Y. Mehmood, S. Ahmed, and R. Mehek, Effect of Co-Ni Ratio in Graphene Based Bimetallic Electro-catalyst for Methanol Oxidation. Fuel Cells. **18**.189-194 (2018). https://doi.org/10.1002/fuce.201700143.

[35] L. Yaqoob, T. Noor, N. Iqbal, H. Nasir, M. Sohail, N. Zaman, et al., Nanocomposites of cobalt benzene tricarboxylic acid MOF with rGO: An efficient and robust electocatalyst for oxygen evaluation reaction (OER). Renew. Energy. **156**. 1040-1054 (2020) https://doi.org/10.1016/j.renene.2020.04.

[36] J. Gao, X. Qian, R. B. Lin, R. Krishna, H. Wu, W. Zhou, et al., Mixed metal–organic framework with multiple binding sites for efficient C2H2/CO2 separation. Angew.Chem.Int.Ed. **59**. 4396-4400 (2020). https://doi.org/10.1002/anie.202000323.

[37] C. O. Ania, M. Seredych, E. Rodriguez-Castellon, and T. J. Bandosz, New copper/GO based material as an efficient oxygen reduction catalyst in an alkaline medium: The role of unique Cu/rGO architecture. Appl.Catal B: Environ. **163.** 424-435 (2015). https://doi.org/10.1016/j.apcatb.2014.08.022.

[38] T. Noor, N. Iqbal, H. Nasir, N. Zaman, and K. Talha, Electrochemical synergies of Fe–Ni bimetallic MOF CNTs catalyst for OER in water splitting. J alloy Compd. **850**. 156583 (2020). https://doi.org/10.1016/j.jallcom.2020.156583.

[39] X. Li, H. Lei, C. Yang, and Q. Zhang, Electrochemical fabrication of ultra-low loading Pt decorated porous nickel frameworks as efficient catalysts for methanol electrooxidation in alkaline medium. J. Power Sources. **396**. 64-72 (2018). https://doi.org/10.1016/j.jpowsour.2018.06.016.

[40] L. Guerrero-Ortega, A. Manzo-Robledo, E. Ramírez-Meneses, J. Mateos-Santiago, L. Lartundo-Rojas, and V. Garibay-Febles, Methanol electro-oxidation reaction at the interface of (bi)-metallic (PtNi) synthesized nanoparticles supported on carbon Vulcan. Int. j. Hydrog.Energy. **43**. 6117-6130 (2018). https://doi.org/10.1016/j.ijhydene.2018.02.003.

[41] D. M. Ferrer, J. A. M. Banda, R. S. Rodrigo, J. Y. V. Gómez, U. P. García, P. D. Á. Vicente, et al., Electrochemical Performance of Pt/NC and Pt/rGO for Methanol Oxidation in Acid Media,ECS Trans. **84.** 41 (2018). https://doi.org/10.1149/08401.0041ecst.

[42] X. Li, L. Luo, F. Peng, H. Wang, and H. Yu, Enhanced activity of Pt/CNTs anode catalyst for direct methanol fuel cells using Ni2P as co-catalyst. Appl.Surf. Sci. **434**. 534-539 (2018). https://doi.org/10.1016/j.apsusc.2017.10.218.

[43] J. Li, Z. Luo, Y. Zuo, J. Liu, T. Zhang, P. Tang, et al., NiSn bimetallic nanoparticles as stable electrocatalysts for methanol oxidation reaction. Appl. Catal. B: Environ. **234**.10-18 (2018). https://doi.org/10.1016/j.apcatb.2018.04.017.

[44] M. B. Askari, M. Seifi, S. M. Rozati, and A. Beheshti-Marnani, One-step hydrothermal synthesis of MoNiCoS nanocomposite hybridized with graphene oxide as a high-performance nanocatalyst toward methanol oxidation. Chem. Phys. Letters. **706.** 164-169 (2018). https://doi.org/10.1016/j.cplett.2018.05.066.

[45] Y. Wang, C. Liu, J. Xiang, L. Xing, X. Ou, S. Chen, et al., Electrocatalytic Oxidation of Methanol on Nickel Doped Metal-Organic Frameworks MIL-110 Modified Glassy Carbon

Electrode in Alkaline Medium. Int. J. Electrochem. Sci. **14.** 5247-5258 (2019).http:// doi: 10.20964/2019.06.11.

[46] S. Hussain, N. Ullah, Y. Zhang, A. Shaheen, M. S. Javed, L. Lin, et al., One-step synthesis of unique catalyst Ni9S8@ C for excellent MOR performances. Int.J. Hydrog. Energy. **44**. 24525-24533 (2019). https://doi.org/10.1016/j.ijhydene.2019.07.190.

[47] S. Wei, L. Qian, D. Jia, and Y. Miao, Synthesis of 3D Flower-Like Ni 0.6 Zn 0.4 O Microspheres for Electrocatalytic Oxidation of Methanol, Electrocatalysis. **10.** 540-548 (2019). https://doi.org/10.1007/s12678-019-00542-5.

[48] S. J. Hoseini, M. Bahrami, and S. M. Nabavizadeh, ZIF-8 nanoparticles thin film at an oil–water interface as an electrocatalyst for the methanol oxidation reaction without the application of noble metals. New J. Chem. vol. **43.** 15811-15822 (2019). https://doi.org/10.1039/C9NJ02855B.

[49] J. Lan, C. Li, T. Liu, and Q. Yuan, One-step synthesis of porous PtNiCu trimetallic nanoalloy with enhanced electrocatalytic performance toward methanol oxidation. j.Saudi Chem. Soc. **23**. 43-51 (2019). https://doi.org/10.1016/j.jscs.2018.04.002.

[50] Y. Liu, B. Hu, S. Wu, M. Wang, Z. Zhang, B. Cui, et al., Hierarchical nanocomposite electrocatalyst of bimetallic zeolitic imidazolate framework and MoS2 sheets for non-Pt methanol oxidation and water splitting. Appl.Catal. B: Environ. **258.** 117970 (2019). https://doi.org/10.1016/j.apcatb.2019.117970.

[51] L. Yaqoob, T. Noor, N. Iqbal, H. Nasir, and N. Zaman, Development of nickel-BTC-MOF-derived nanocomposites with rGO towards electrocatalytic oxidation of methanol and its product analysis. Catalysts. **9.** 856 (2019). https://doi.org/10.3390/catal9100856.

[52] S. L. Candelaria, N. M. Bedford, T. J. Woehl, N. S. Rentz, A. R. Showalter, S. Pylypenko, et al., Multi-component Fe–Ni hydroxide nanocatalyst for oxygen evolution and methanol oxidation reactions under alkaline conditions. ACS Catal. **7**. 365-379 (2017). https://doi.org/10.1021/acscatal.6b02552.

[53] B. Iqbal, M. Saleem, S. N. Arshad, J. Rashid, N. Hussain, and M. Zaheer, One-pot Synthesis of Heterobimetallic Metal-Organic Frameworks (MOF) for Multifunctional Catalysis. Chem.Eur.J. **25**. 10490-10498 (2019). https://doi.org/.1002/chem.201901939.

[54] Z.-S. Wu, W. Ren, L. Gao, B. Liu, C. Jiang, and H.-M. Cheng, Synthesis of high-quality graphene with a pre-determined number of layers," Carbon, vol. 47, pp. 493-499, 2009.

[55] N. Cao and Y. Zhang, Study of reduced graphene oxide preparation by Hummers' method and related characterization. J. Nanomate. **2015**. 108 (2015). https://doi.org/10.1155/2015/168125.

[56] B. Wu, X. Lin, L. Ge, L. Wu, and T. Xu, A novel route for preparing highly proton conductive membrane materials with metal-organic framework.Chem. Commun.**49.**143-145 (2013). https://doi.org/10.1039/C2CC37045J.

[57] T. A. Vu, G. H. Le, C. D. Dao, L. Q. Dang, K. T. Nguyen, P. T. Dang, et al.,Isomorphous substitution of Cr by Fe in MIL-101 framework and its application as a novel heterogeneous photo-Fenton catalyst for reactive dye degradation. RSC Adv. **4**. 41185-41194 (2014). https://doi.org/10.1039/C4RA06522K.

[58] H. Guo, Z. Zheng, Y. Zhang, H. Lin, and Q. Xu, Highly selective detection of Pb2+ by a nanoscale Ni-based metal–organic framework fabricated through one-pot hydrothermal reaction.Sens.ActuatorsB:Chem.**248**.430-436(2017). https://doi.org/10.1016/j.snb.2017.03.147.

[59] A. Mesbah, P. Rabu, R. Sibille, S. Lebègue, T. Mazet, B. Malaman, et al., From hydrated Ni3 (OH) 2 (C8H4O4) 2 (H2O) 4 to anhydrous Ni2 (OH) 2 (C8H4O4): impact of structural transformations on magnetic properties. Inorg. Chem. **53**. 872-881 (2014). https://doi.org/10.1021/ic402106v.

[60] Z. Zhang, X. Li, B. Liu, Q. Zhao, and G. Chen, Hexagonal microspindle of NH 2-MIL-101 (Fe) metal–organic frameworks with visible-light-induced photocatalytic activity for the degradation of toluene. Rsc Adv. **6.** 4289-4295 (2016). https://doi.org/10.1039/C5RA23154J.

[61] P. Arul and S. A. John, Size controlled synthesis of Ni-MOF using polyvinylpyrrolidone: New electrode material for the trace level determination of nitrobenzene. J. Electroanal. Chem. **829**. 168-176 (2018). https://doi.org/10.1016/j.jelechem.2018.10.014.

[62] G.-T. Vuong, M.-H. Pham, and T.-O. Do, Synthesis and engineering porosity of a mixed metal Fe 2 Ni MIL-88B metal–organic framework. Dalton Trans. **42**. 550-557 (2013). https://doi.org/10.1039/C2DT32073H.

[63] T. Iwasaki, H. Yoshii, H. Nakamura, and S. Watano, Simple and rapid synthesis of Ni–Fe layered double hydroxide by a new mechanochemical method. App. clay Sci. **58**. 120-124 (2012). https://doi.org/10.1016/j.clay.2012.01.024.

[64] L. Zhou, X. Kong, M. Gao, F. Lian, B. Li, Z. Zhou, et al., Hydrothermal fabrication of MnCO3@ rGO composite as an anode material for high-performance lithium ion batteries. Inorg. Chem. **53**. 9228-9234 (2014). https://doi.org/10.1021/ic501321z.

[65] F. Israr, D. K. Kim, Y. Kim, S. J. Oh, K. C. Ng, and W. Chun, Cost effective and low energy consuming hydrothermal synthesis of Ni based MOF. j.Energy Eng**. 24.** 51-54 (2015). https://doi.org/10.5855/ENERGY.2015.24.2.051.

[66] Z. Wang, P. Dong, Z. Sun, C. Sun, H. Bu, J. Han, et al., Sizes/morphologies tunable NH2-Ni-MOFs electrocatalysts for ultrasensitive C-reactive protein detection via an aptamer binding induced DNA walker-antibody sandwich assay. J Mater Chem B. **10**. 1039 (2018). https://doi.org/10.1039/C3TA14647B.

[67] Y. Bai, M. Du, J. Chang, J. Sun, and L. Gao, Supercapacitors with high capacitance based on reduced graphene oxide/carbon nanotubes/NiO composite electrodes," J. Mater. Chem A. **2.** 3834-3840 (2014). https://doi.org/10.1039/C3TA15004F.

[68] K. Lian, D. Kirk, and S. Thorpe, Investigation of a "Two-State" Tafel Phenomenon for the Oxygen Evolution Reaction on an Amorphous Ni-Co Alloy. J. Electrochem. Soc. **142.** 3704 (1995). https://doi.org/10.1149/1.2048402.

[69] T. J. Siang, L. G. Bach, S. Singh, Q. D. Truong, N. H. H. Phuc, F. Alenazey, et al., Methane bi-reforming over boron-doped Ni/SBA-15 catalyst: Longevity evaluation. Int. J. Hydrog.Energy. **44**. 20839-20850 (2019). https://doi.org/10.1016/j.ijhydene.2018.06.123.

[70] Z. Wang, P. Dong, Z. Sun, C. Sun, H. Bu, J. Han, et al.,NH2-Ni-MOF electrocatalysts with tunable size/morphology for ultrasensitive C-reactive protein detection via an aptamer binding induced DNA walker–antibody sandwich assay. J. Mater. Chem B. **6**. 2426-2431 (2018). https://doi.org/10.1039/C8TB00373D.

[71] K. Fominykh, J. M. Feckl, J. Sicklinger, M. Döblinger, S. Böcklein, J. Ziegler, et al., Ultrasmall dispersible crystalline nickel oxide nanoparticles as high-performance catalysts for electrochemical water splitting. Adv. Funct. Mater**. 24.** 3123-3129 (2014). https://doi.org/10.1002/adfm.201303600.

[72] X.-Y. Yu, Y. Feng, B. Guan, X. W. D. Lou, and U. Paik, Carbon coated porous nickel phosphides nanoplates for highly efficient oxygen evolution reaction. Energ Environ. Sci. **9.** 1246-1250 (2016). https://doi.org/10.1039/C6EE00100A.

[73] Z. Wang, P. Dong, Z. Sun, C. Sun, H. Bu, J. Han, et al., NH 2-Ni-MOF electrocatalysts with tunable size/morphology for ultrasensitive C-reactive protein detection via an aptamer binding induced DNA walker–antibody sandwich assay. J. Mater.Chem B. **6**. 2426-2431 (2018). https://doi.org/10.1039/C8TB00373D.

[74] L. Zhang, Y. Hashimoto, T. Taishi, and Q.-Q. Ni, Mild hydrothermal treatment to prepare highly dispersed multi-walled carbon nanotubes. Appl. Surf. Sci. **257**. 1845-1849 (2011). https://doi.org/10.1016/j.apsusc.2010.08.106.

[75] G. J. H. Melvin, Q.-Q. Ni, Y. Suzuki, and T. Natsuki, Microwave-absorbing properties of silver nanoparticle/carbon nanotube hybrid nanocomposites. J. Mater. Sci**. 49**. 5199-5207 (2014). https://doi.org/10.1007/s10853-014-8229-9.

[76] S. Santangelo, G. Messina, G. Faggio, M. Lanza, and C. Milone, Evaluation of crystalline perfection degree of multi-walled carbon nanotubes: correlations between thermal kinetic analysis and micro-Raman spectroscopy. J Raman Spectrosc. **42**. 593-602 (2011). https://doi.org/10.1002/jrs.2766.

[77] Y. Lin, K. A. Watson, M. J. Fallbach, S. Ghose, J. G. Smith Jr, D. M. Delozier, et al., Rapid, solventless, bulk preparation of metal nanoparticle-decorated carbon nanotubes. ACS nano. **3**. 871-884 (2009). https://doi.org/10.1021/nn8009097.

[78] P. Corio, A. Santos, P. S. Santos, M. L. A. Temperini, V. Brar, M. A. Pimenta, et al., Characterization of single wall carbon nanotubes filled with silver and with chromium

compounds.Chem.Phys.Letters.**383.**475-480(2004).
https://doi.org/10.1016/j.cplett.2003.11.061.

[79] S. Kumaraguru, J. Yesuraj, and S. Mohan, Reduced graphene oxide-wrapped micro-rod like Ni/Co organic-inorganic hybrid nanocomposite as an electrode material for high-performancesupercapacitor.ComposBEng.**185**.107767(2020).
https://doi.org/10.1016/j.compositesb.2020.107767.

[80] N. Xu, T. Zhu, J. Qiao, F. Zhang, and Z. Chen, Nitrogen and sulfur co-doped mesoporous carbon as cathode catalyst for H2/O2 alkaline membrane fuel cell–effect of catalyst/bonding layer loading. Int. j. hydrog. Eng. **41**. 9159-9166 (2016). https://doi.org/10.1016/j.ijhydene.2015.11.119.

[81] L. Wu, Q. Li, C. H. Wu, H. Zhu, A. Mendoza-Garcia, B. Shen, et al., Stable cobalt nanoparticles and their monolayer array as an efficient electrocatalyst for oxygen evolution reaction. J. Am. Chem. Soc. 1**37**. 7071-7074 (2015). https://doi.org/10.1021/jacs.5b04142.

[82] Y. Fang, X. Li, F. Li, X. Lin, M. Tian, X. Long, et al., Self-assembly of cobalt-centered metal organic framework and multiwalled carbon nanotubes hybrids as a highly active and corrosion-resistant bifunctional oxygen catalyst. J. Power Sources. **326**. 50-59 (2016). https://doi.org/10.1016/j.jpowsour.2016.06.114.

[83] M. Xing, L.-B. Kong, M.-C. Liu, L.-Y. Liu, L. Kang, and Y.-C. Luo, Cobalt vanadate as highly active, stable, noble metal-free oxygen evolution electrocatalyst. J.Mater. Chem A. **2**. 18435-18443 (2014). https://doi.org/10.1039/C4TA03776F.

.[84] E. H. Yu, K. Scott, R. W. Reeve, L. Yang, and R. G. Allen, Characterisation of platinised Ti mesh electrodes using electrochemical methods: methanol oxidation in sodium

hydroxidesolutions.Electrochim.Act.**49**443-2452(2004). https://doi.org/10.1016/j.electacta.2004.01.022.

[85] O. O. Fashedemi and K. I. Ozoemena, Enhanced methanol oxidation and oxygen reduction reactions on palladium-decorated FeCo@ Fe/C core–shell nanocatalysts in alkaline medium. Phys. Chem. Chem. Phys. **15**. 20982-20991 (2013). https://doi.org/10.1039/C3CP52601A.

[86] L. Yaqoob, T. Noor, N. Iqbal, H. Nasir, N. Zaman, L. Rasheed, et al., Development of an Efficient Non-Noble Metal Based Anode Electrocatalyst to Promote Methanol Oxidation Activity in DMFC. Chem. Select. **5**. 6023-6034 (2020). https://doi.doi.org/10.1002/slct.2020

[87] G. Zeng, Y. Chen, L. Chen, P. Xiong, and M. Wei, Hierarchical cerium oxide derived from metal-organic frameworks for high performance supercapacitor electrodes. Electrochim. Acta. **222**. 773-780 (2016). https://doi.org/10.1016/j.electacta.2016.11.035.

[88] L. Hamidipour and F. Farzaneh, Cobalt metal organic framework as an efficient heterogeneous catalyst for the oxidation of alkanes and alkenes," React. Kinet. **109**. 67-75 (2013). https://doi.org/10.1007/s11144-012-0533-2.

[89] S. Parwaiz, K. Bhunia, A. K. Das, M. M. Khan, and D. Pradhan, Cobalt-doped ceria/reduced graphene oxide nanocomposite as an efficient oxygen reduction reaction catalyst and supercapacitor material. J. Phys.Chem C. **121**. 20165-20176 (2017). https://doi.org/10.1021/acs.jpcc.7b06846.

[90] Y. Li, G. Wang, K. Ye, K. Cheng, Y. Pan, P. Yan, et al., Facile preparation of three-dimensional multilayer porous MnO2/reduced graphene oxide composite and its

supercapacitive performance. J. Power Sources.**271**. 582-588(2014). https://doi.org/10.1016/j.jpowsour.2014.08.048.

[91] V. Maruthapandian, S. Kumaraguru, S. Mohan, V. Saraswathy, and S. Muralidharan, An insight on the electrocatalytic mechanistic study of pristine Ni MOF (BTC) in alkaline medium for enhanced OER and UOR. ChemElectroChem. **5**. 2795-2807 (2018). https://doi.org/10.1002/celc.201800802.

[92] C. Cordeiro, M. De Vries, T. Cremers, and B. Westerink, The role of surface availability in membrane-induced selectivity for amperometric enzyme-based biosensors, Sens. Actuat atorB: Chem. **223**. 679-688 (2016). https://doi.org/10.1016/j.snb.2015.09.029.

[93] M. M. Shahid, A. Pandikumar, A. M. Golsheikh, N. M. Huang, and H. N. Lim, Enhanced electrocatalytic performance of cobalt oxide nanocubes incorporating reduced graphene oxide as a modified platinum electrode for methanol oxidation. RSC Adv .**4**. 62793-62801 (2014). https://doi.org/10.1039/C4RA08952A.

[94] S. Devaraj and N. Munichandraiah, Electrochemical supercapacitor studies of nanostructured α-MnO2 synthesized by microemulsion method and the effect of annealing. J. Electrochem. Soc. **154**. 80 (2006). https://doi.org/10.1149/1.2404775.

[95] L. Niu, Q. Li, F. Wei, X. Chen, and H. Wang, Electrochemical impedance and morphological characterization of platinum-modified polyaniline film electrodes and their electrocatalytic activity for methanol oxidation. J. Electroanal. Chem. **544**. 121-128 (2003). https://doi.org/10.1016/S0022-0728(03)00085-8.

[96] X. Zhu, P. Zhang, S. Xu, X. Yan, and Q. Xue, Free-standing three-dimensional graphene/manganese oxide hybrids as binder-free electrode materials for energy storage

applications. ACS Appl. Mater. Interfaces. **6**. 11665-11674 (2014). https://doi.org/10.1021/am5024258.

[97] Q. Wu, M. Jiang, X. Zhang, J. Cai, and S. Lin, A novel octahedral MnO/RGO composite prepared by thermal decomposition as a noble-metal free electrocatalyst for ORR. J. Mater. Sci. **52**. 6656-6669 (2017). https://doi.org/10.1007/s10853-017-0901-4.

[98] E. H. Yu, K. Scott, and R. W. Reeve, A study of the anodic oxidation of methanol on Pt in alkaline solutions. J. Electroanal. Chem. **547**. 17-24 (2003). https://doi.org/10.1016/S0022-0728(03)00172-4.

[99] W. Ye, X. Zhang, Y. Chen, Y. Du, F. Zhou, and C. Wang, Pulsed electrodeposition of reduced graphene oxide on glass carbon electrode as an effective support of electrodeposited Pt microspherical particles: nucleation studies and the application for methanol electro-oxidation. Int. J. Electrochem. Sci. . **8**. 2122-2139 (2013).

[100] T. Huang, S. Mao, G. Zhou, Z. Zhang, Z. Wen, X. Huang, et al., A high-performance catalyst support for methanol oxidation with graphene and vanadium carbonitride. Nanoscale. **7**. 1301-1307 (2015). https://doi.org/10.1039/C4NR05244G.

[101] W. Wang, Y. Li, and H. Wang, Tin oxide nanoparticle-modified commercial PtRu catalyst for methanol oxidation. Micro Nano Lett. **8**. 23-26 (2013). https://doi.org/10.1049/mnl.2012.0774.

[102] Y. Huang, J. Cai, M. Liu, and Y. Guo, Fabrication of a novel PtPbBi/C catalyst for ethanol electro-oxidation in alkaline medium. Electrochim. Act. **83**. 1-6 (2012). https://doi.org/10.1016/j.electacta.2012.07.089.

[103] H. Wang, H. Da, R. Wang, and S. Ji, Beef-derived mesoporous carbon as highly efficient support for PtRuIr electrocatalysts and their high activity for CO and methanol oxidation. S. Afr. J. Chem. **67**. 33–39 (2014).

[104] W. Ye, X. Zhang, Y. Chen, Y. Du, F. Zhou, and C. Wang, Electrodeposition of reduced graphene oxide on glass carbon electrode as an effective support of electrodeposited Pt microspherical particles: nucleation studies and the application for methanol electro-oxidation.Int.J.Electrochem.Sci.**7**.2139(2015). https://doi.org/10.9734/BJAST/2015/16808

[105] H. Wang, V. Linkov, S. Ji, W. Zhang, Z. Lei, and R. Wang, Highly active, carbon-supported, PdSn nano-core, partially covered with Pt, as catalysts for methanol oxidation. S. Afr. J. Chem. **65**. 69-74 (2012). http://journals.sabinet.co.za/sajchem.

[106] S. Mao, Z. Wen, T. Huang, Y. Hou, and J. Chen, High-performance bi-functional electrocatalysts of 3D crumpled graphene–cobalt oxide nanohybrids for oxygen reduction and evolution reactions. Energ. Environ. Sci. **7**. 609-616 (2014). https://doi.org/10.1039/C3EE42696C.

[107] W. Huang, H. Wang, J. Zhou, J. Wang, P. N. Duchesne, D. Muir, et al., Highly active and durable methanol oxidation electrocatalyst based on the synergy of platinum–nickel hydroxide–graphene. Nat. commun . **6**, 10035 (2015). https://doi.org/10.1038/ncomms10035.

[108] G. Behmenyar and A. N. Akın, Investigation of carbon supported Pd–Cu nanoparticles as anode catalysts for direct borohydride fuel cell. J. Power Sources. **249**. 239-246 (2014). https://doi.org/10.1016/j.jpowsour.2013.10.063

[109] Y. Zheng, H. Chen, Y. Dai, N. Zhang, W. Zhao, S. Wang, et al., Preparation and characterization of Pt/TiO2 nanofibers catalysts for methanol electro-oxidation. Electrochim. Acta. **178** . 74-79 (2015). https://doi.org/10.1016/j.electacta.2015.07.177.

[110] M. Jafarian, M. Mahjani, H. Heli, F. Gobal, H. Khajehsharifi, and M. Hamedi, A study of the electro-catalytic oxidation of methanol on a cobalt hydroxide modified glassy carbon electrode. Electrochim. Acta. **48**. 3423-3429 (2003). https://doi.org/10.1016/S0013-4686(03)00399-2.

[111] H. Sun, Y. Ye, J. Liu, Z. Tian, Y. Cai, P. Li, et al., Pure Ni nanocrystallines anchored on rGO present ultrahigh electrocatalytic activity and stability in methanol oxidation. Chem. Commun. **54**. 1563-1566 (2018). https://doi.org/10.1039/C7CC09361F.

[112] M. Sunitha, N. Durgadevi, A. Sathish, and T. Ramachandran, Performance evaluation of nickel as anode catalyst for DMFC in acidic and alkaline medium. J. Fuel Chem.Technol. **46**. 592-599 (2018). https://doi.org/10.1016/S1872-5813(18)30026-4.

[113] J. B. Raoof, R. Ojani, and S. R. Hosseini, An electrochemical investigation of methanol oxidation on nickel hydroxide nanoparticles. S. Afr. J . Chem. **66**. 47-53. (2013). http://journals.sabinet.co.za/sajchem.

[114] C. C. McCrory, S. Jung, J. C. Peters, and T. F. Jaramillo, Benchmarking heterogeneous electrocatalysts for the oxygen evolution reaction. J. Am. Chem. Soc. **135.** 16977-16987 (2013). https://doi.org/10.1021/ja407115p.

[115] Y. Li, W. Gao, L. Ci, C. Wang, and P. M. Ajayan, Catalytic performance of Pt nanoparticles on reduced graphene oxide for methanol electro-oxidation. Carbon. **48**. 1124-1130 (2010). https://doi.org/10.1021/ja407115p.

[116] S. Gamil, W. M. El Rouby, M. Antuch, and I. Zedan, Nanohybrid layered double hydroxide materials as efficient catalysts for methanol electrooxidation. RSC adv. **9**. 13503-13514 (2019). https://doi.org/10.1039/C9RA01270B.

Figures

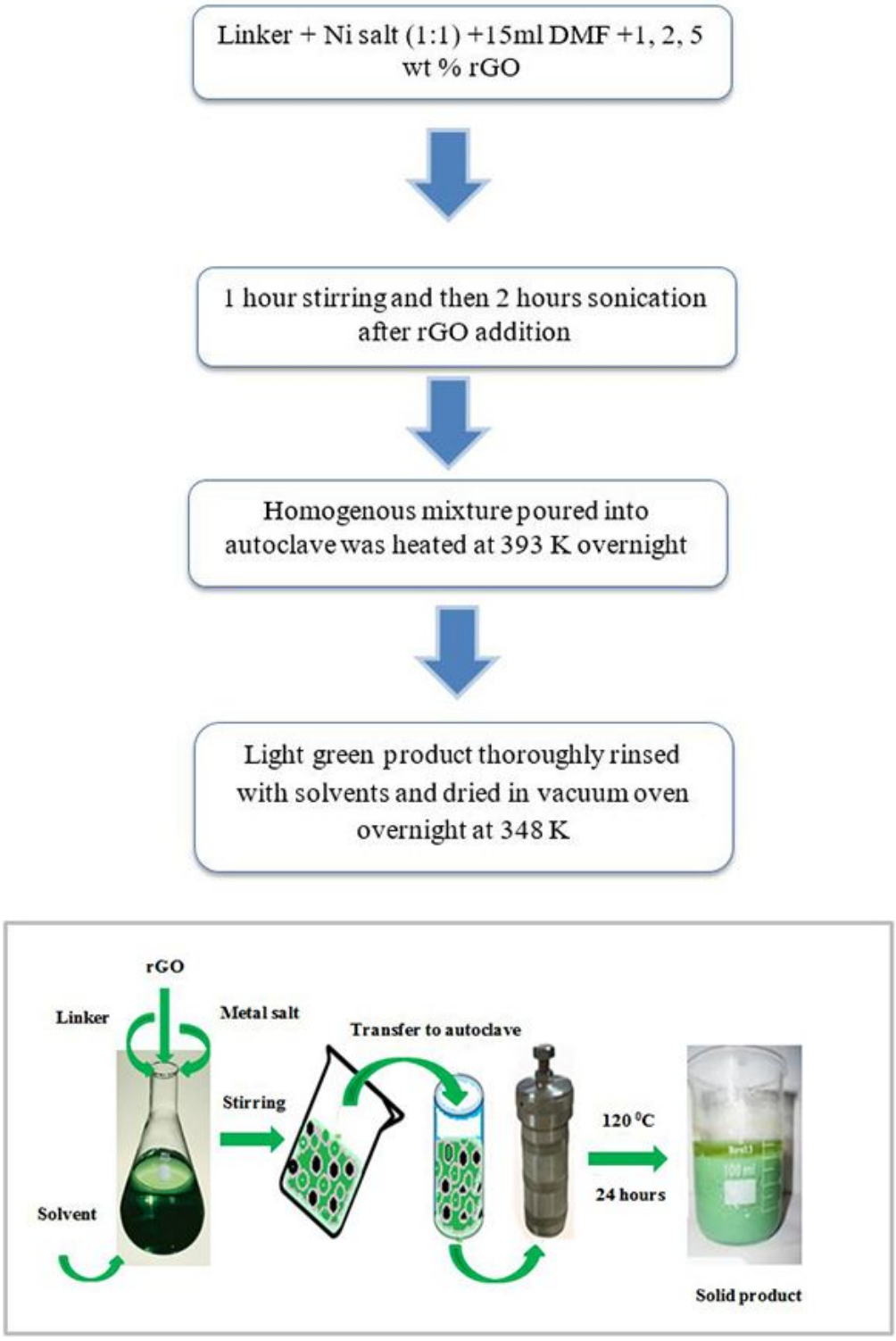

Figure 1

Stepwise synthetic scheme of NiNH2BDC MOF /1, 2, 5 wt % reduced graphitic carbon hybrids and flow sheet diagram for the synthesis of NiNH2BDC MOF/1, 2, 5 wt % reduced graphitic carbon hybrids.

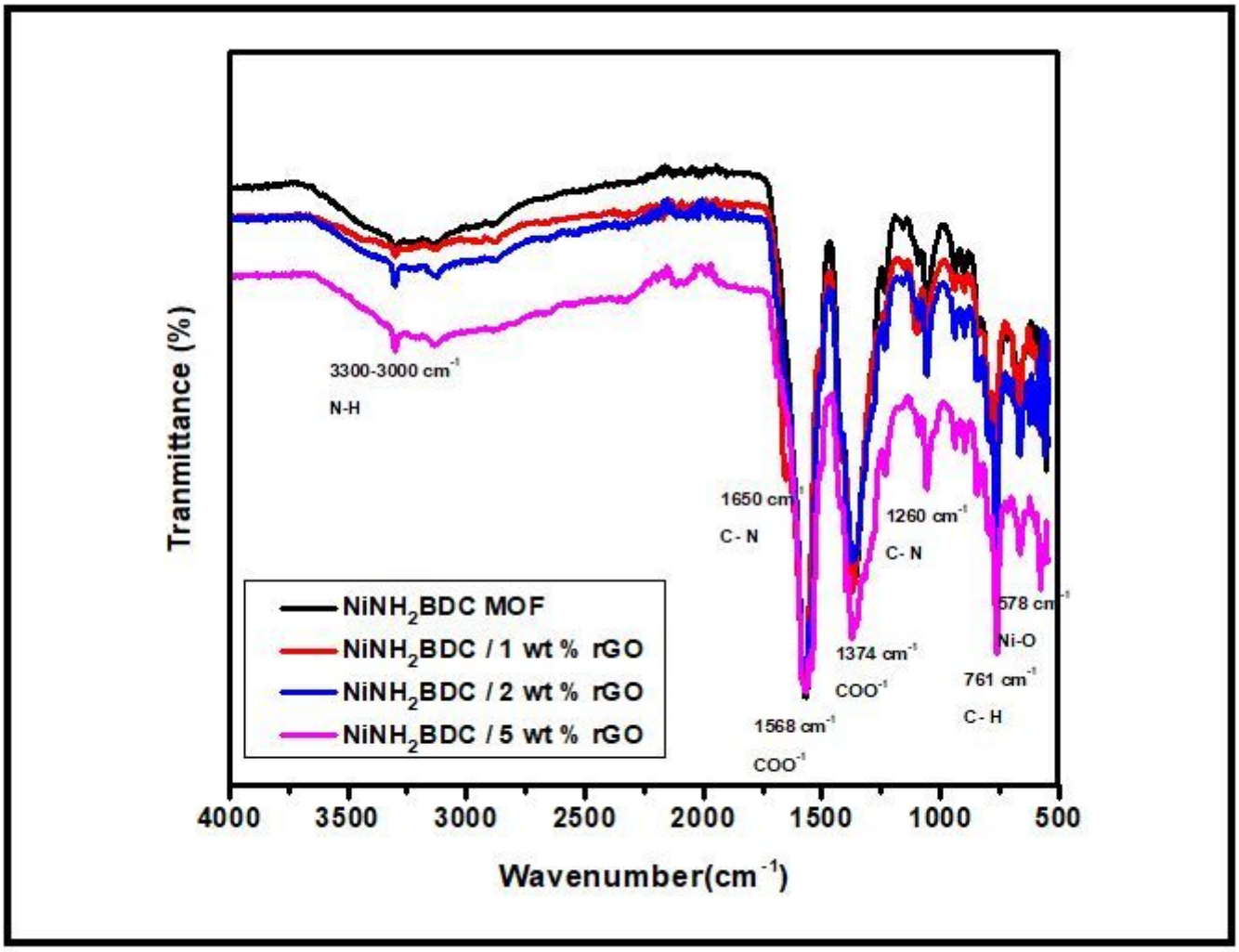

Figure 2

Fourier transformed infrared spectrum of NiNH2BDC MOF/1, 2, 5 wt % reduced graphitic carbon hybrids.

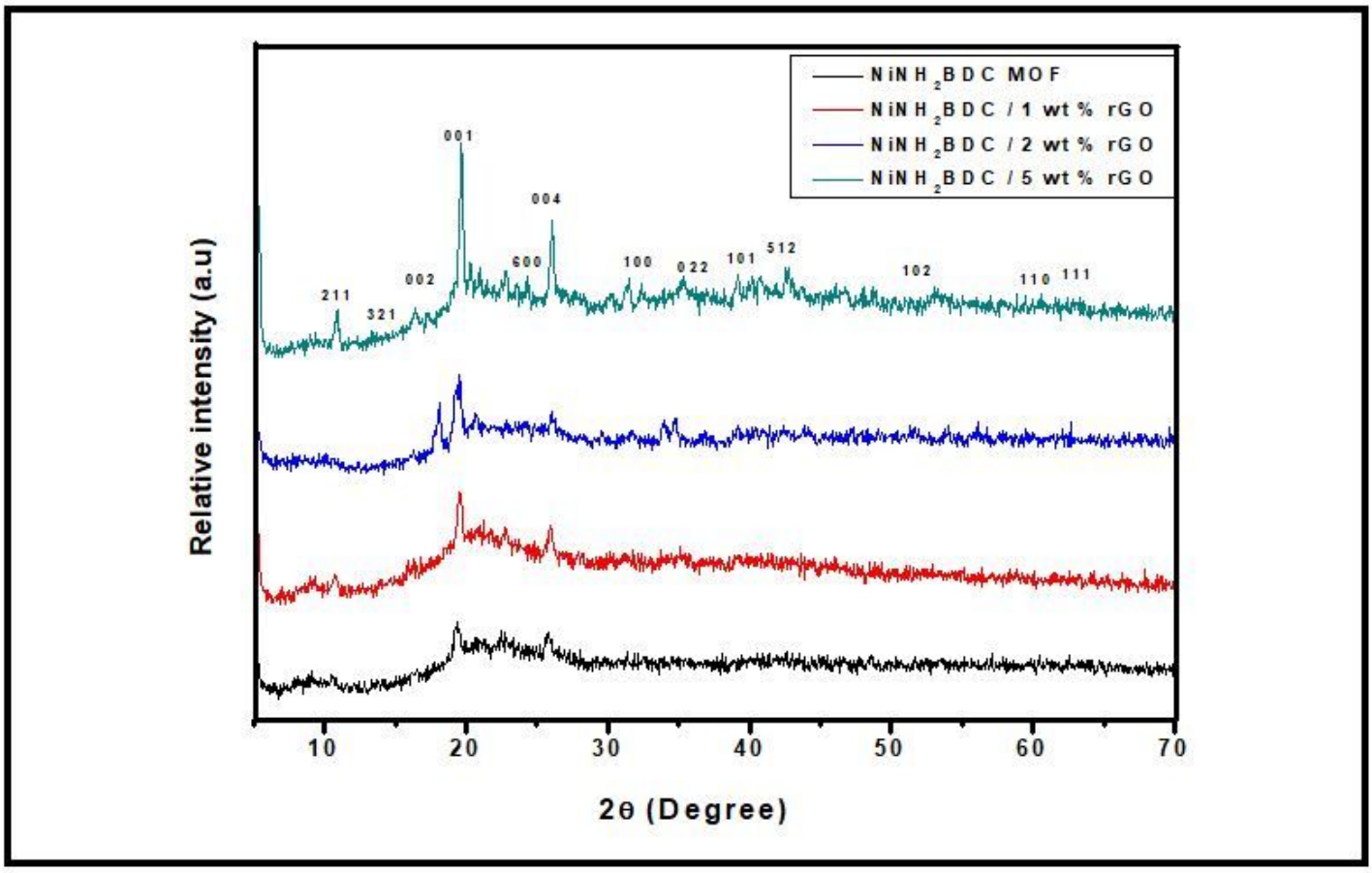

Figure 3

X-ray diffraction pattern of NiNH2BDC MOF/1, 2, 5 wt % reduced graphitic carbon hybrids.

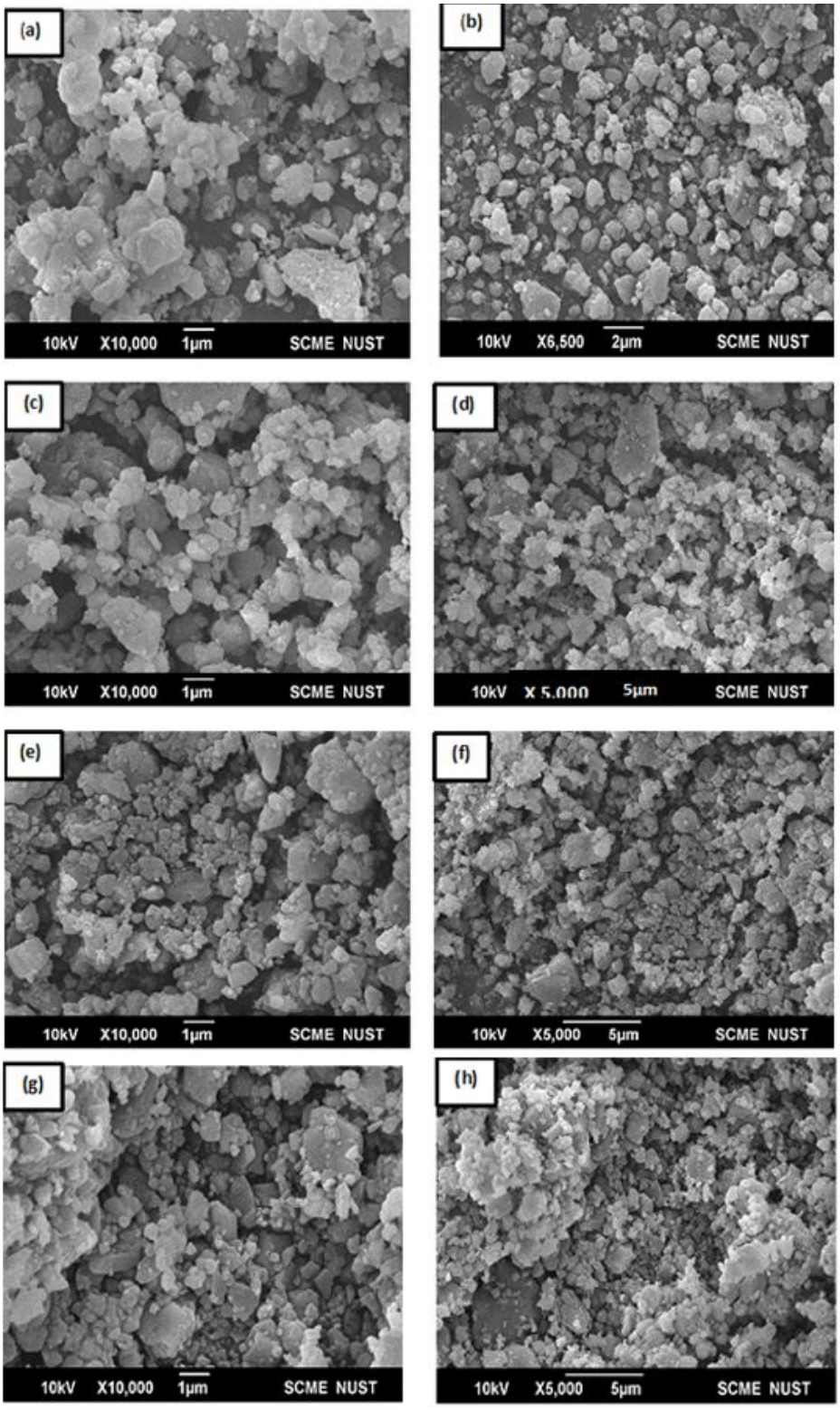

Figure 4

Scanning electron microscopy images of NiNH2BDC MOF (4a,4b), 1wt % rGO composite (4c,4d), 2 wt % rGO composite (4e,4f), and 5 wt % rGO composite (4g,4h) at different magnifications.

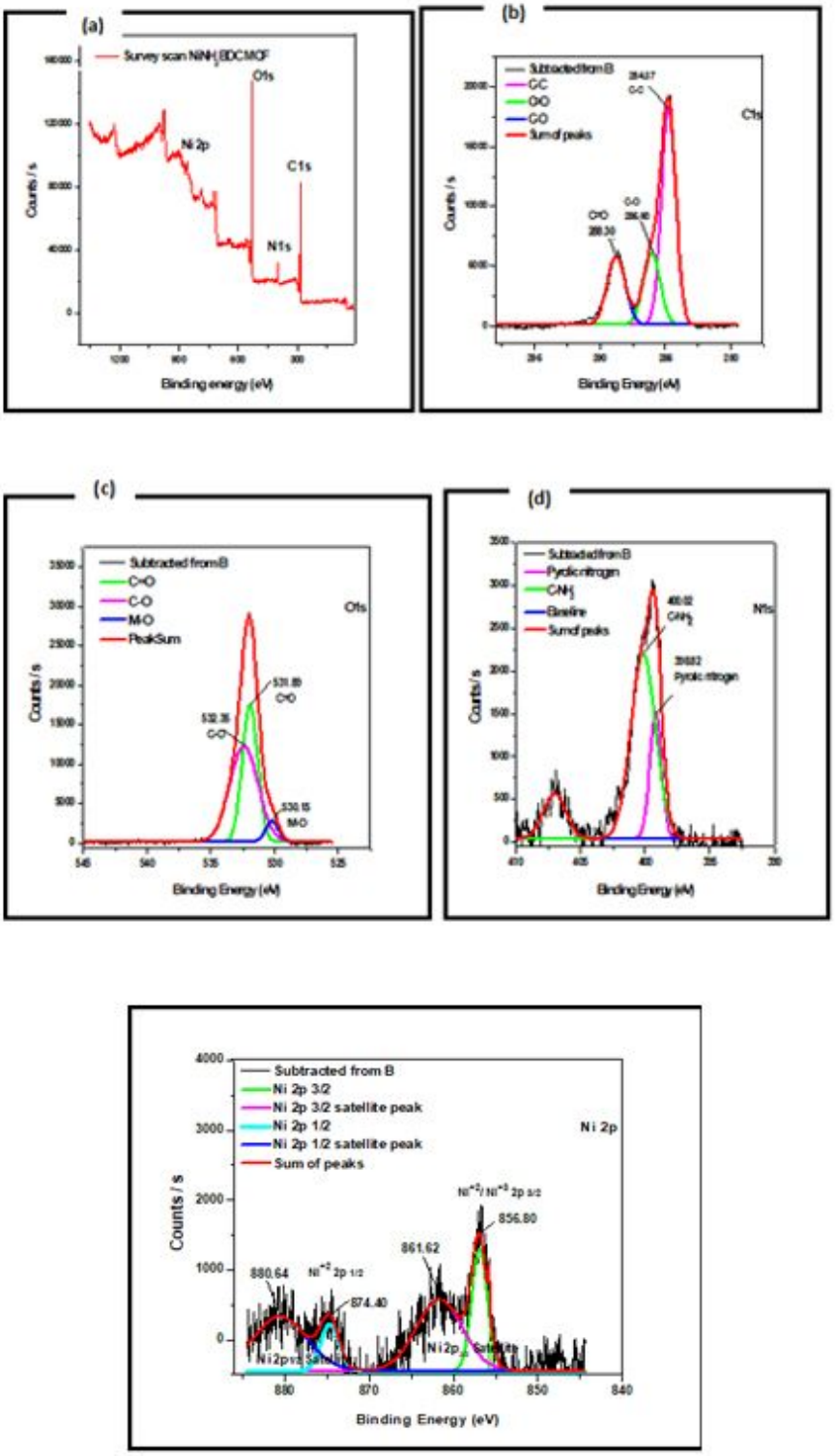

Figure 5

X-ray photoelectron spectra of NiNH2BDC (a) Survey scan (b) Carbon (c) Oxygen (d) Nitrogen, and (e) Nickel.

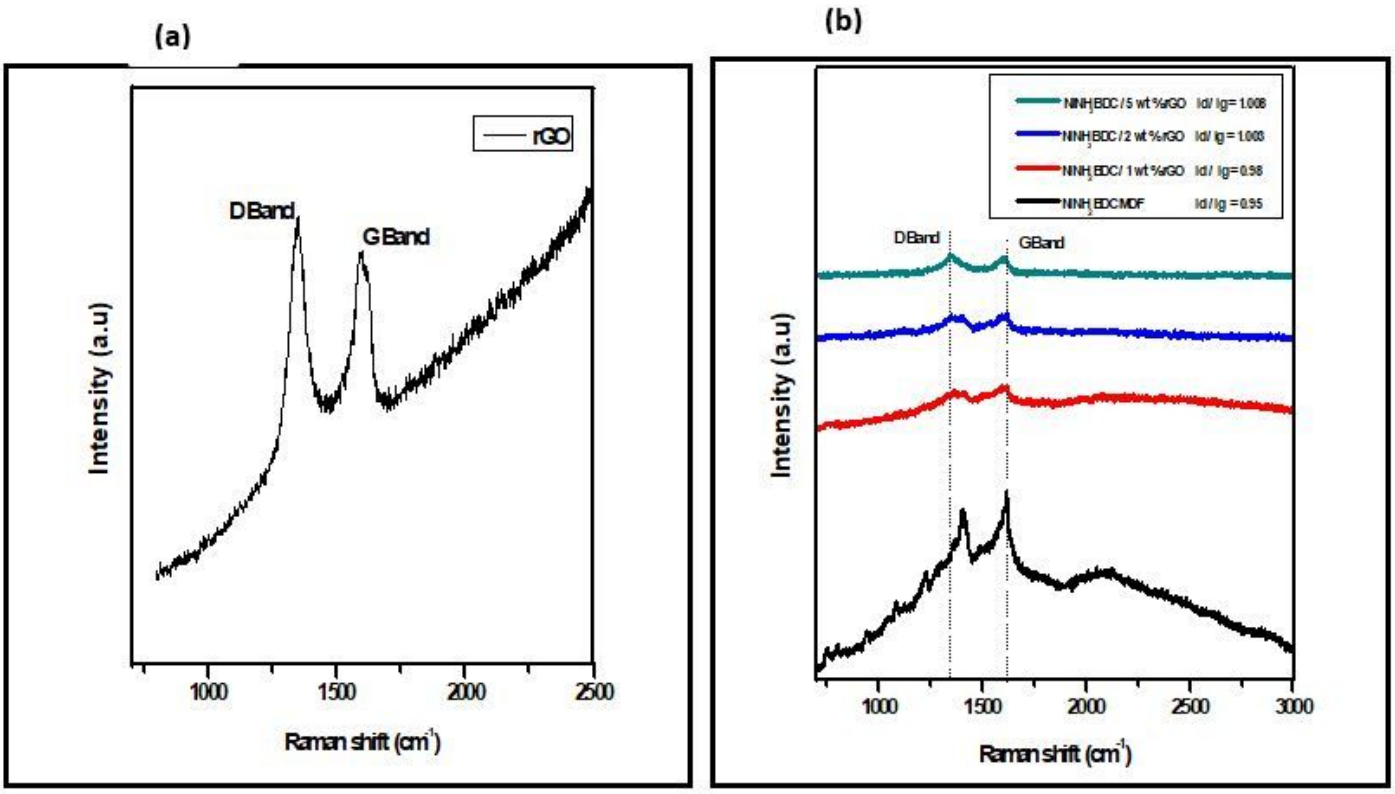

Figure 6

Raman spectra of (a) rGO (b) NiNH2BDC MOF/1, 2, 5 wt % reduced graphitic carbon hybrids.

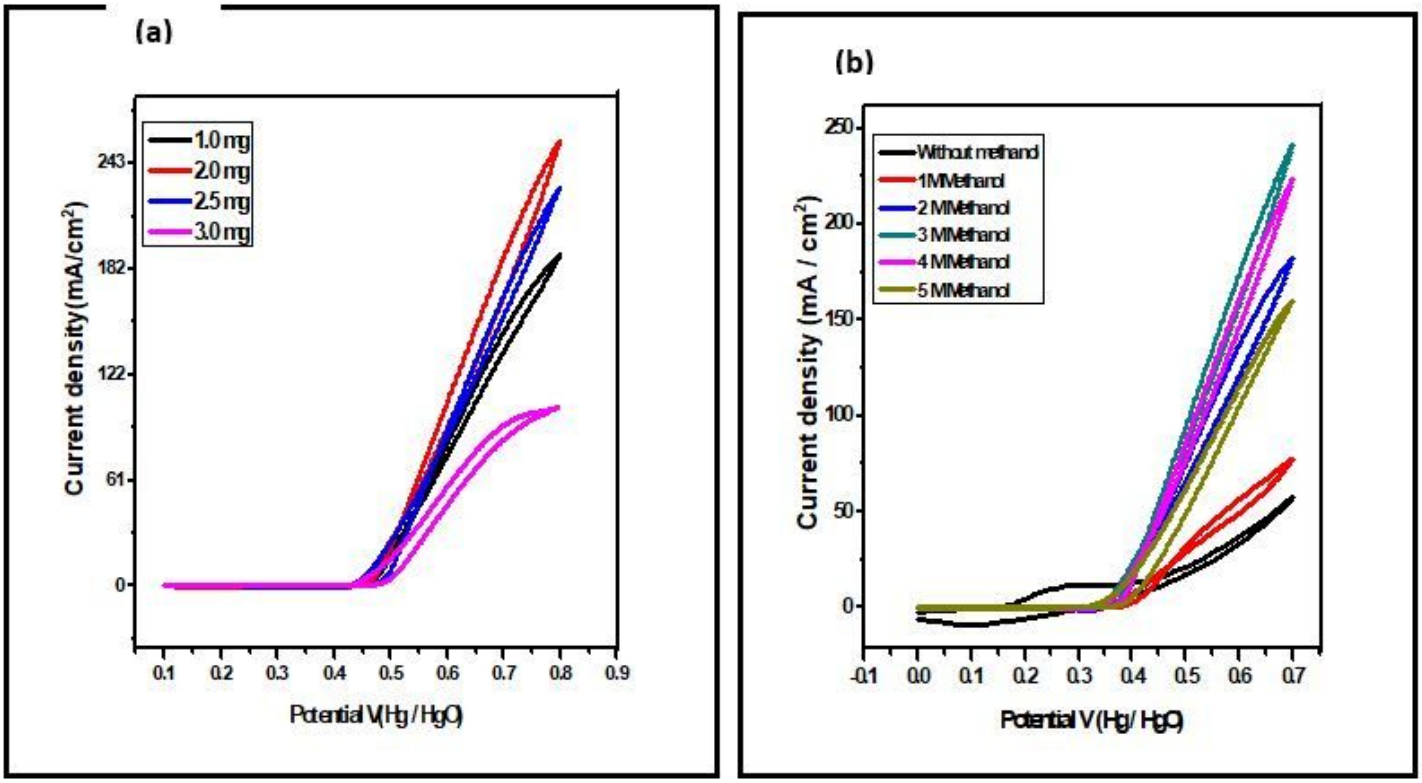

Figure 7

(a) Influence of electrocatalyst deposited quantity, and (b) CH3OH molarity on the current density response of NiNH2BDC MOF/1, 2, 5 wt % reduced graphitic carbon hybrids during the optimization process.

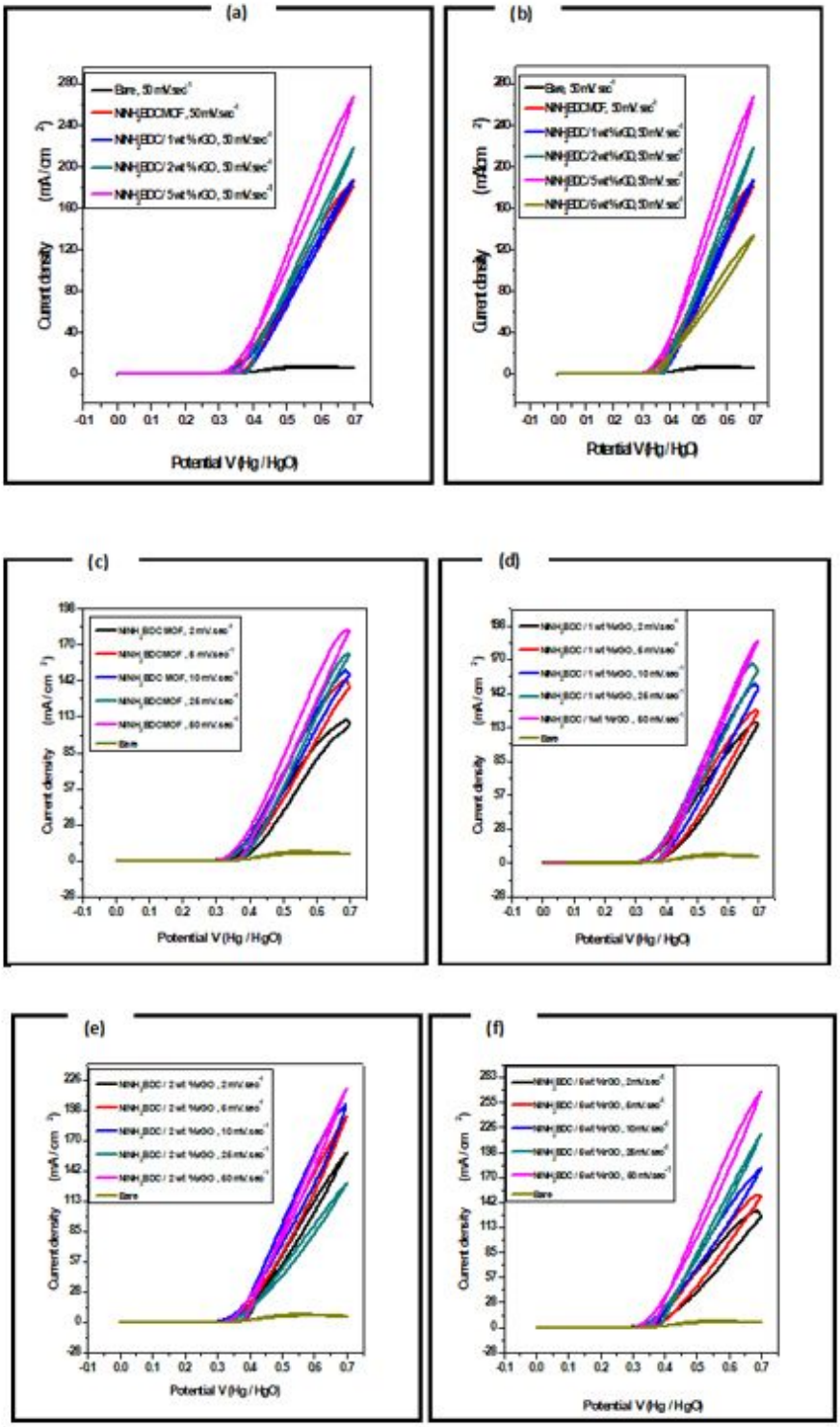

Figure 8

Cyclic voltamogram of (a) NiNH2BDC MOF/1-5 wt % reduced graphitic carbon hybrids at 50 mV/ sec (b) NiNH2BDC MOF/1-6 wt % reduced graphitic carbon hybrids at 50 mV/ sec (c) NiNH2BDC MOF (d) NiNH2BDC/1 wt % reduced graphitic carbon hybrids (e) NiNH2BDC/2 wt % reduced graphitic carbon hybrids, and (f) NiNH2BDC/5 wt % reduced graphitic carbon hybrids in 3 M CH3OH /1 M NaOH solution at scanning speed 2–50 mV/sec.

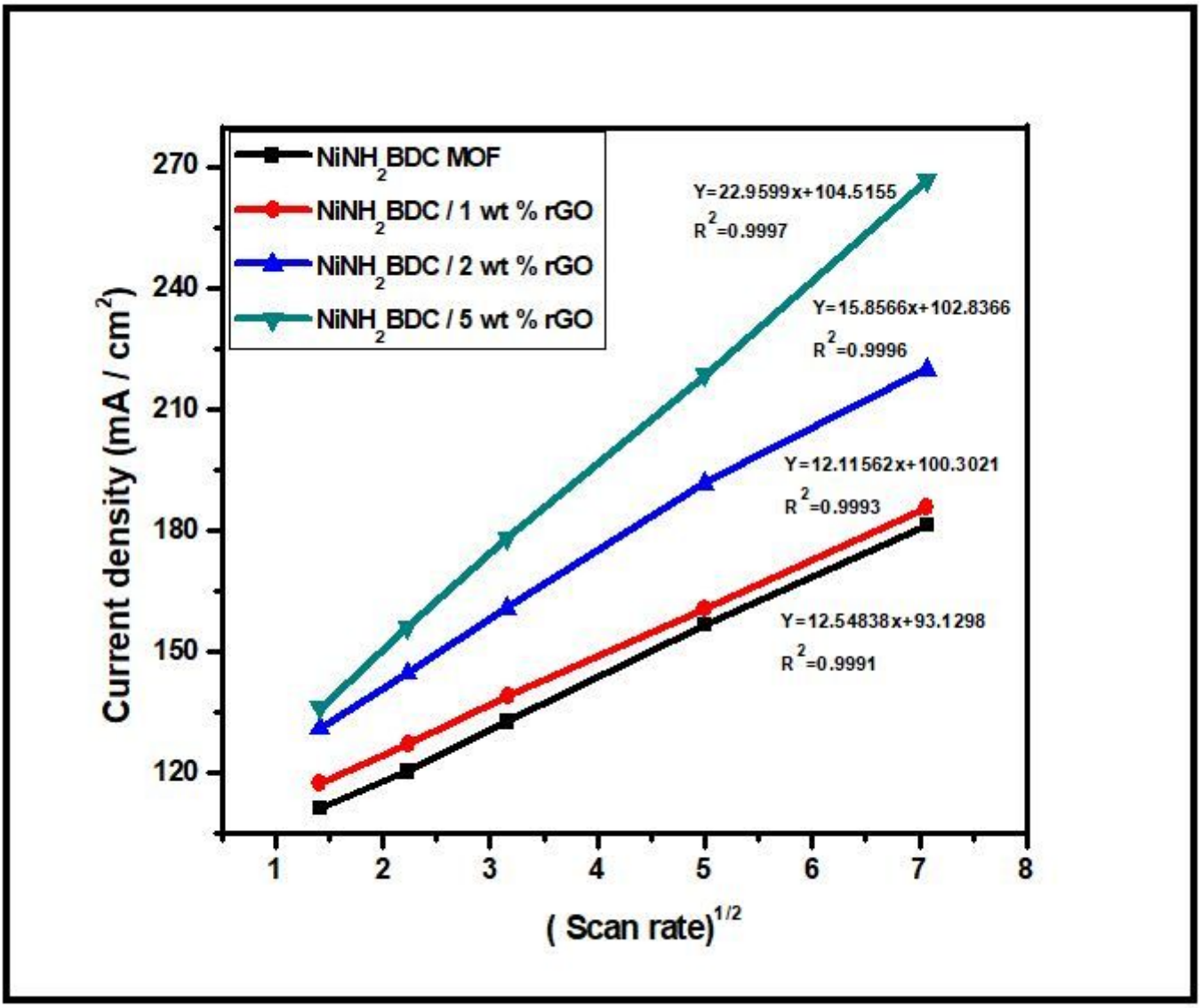

Figure 9

A graphical representation of the direct relationship of peak current density (j) vs under root of scan rate (v) in 3M CH3OH/1 M NaOH solution.

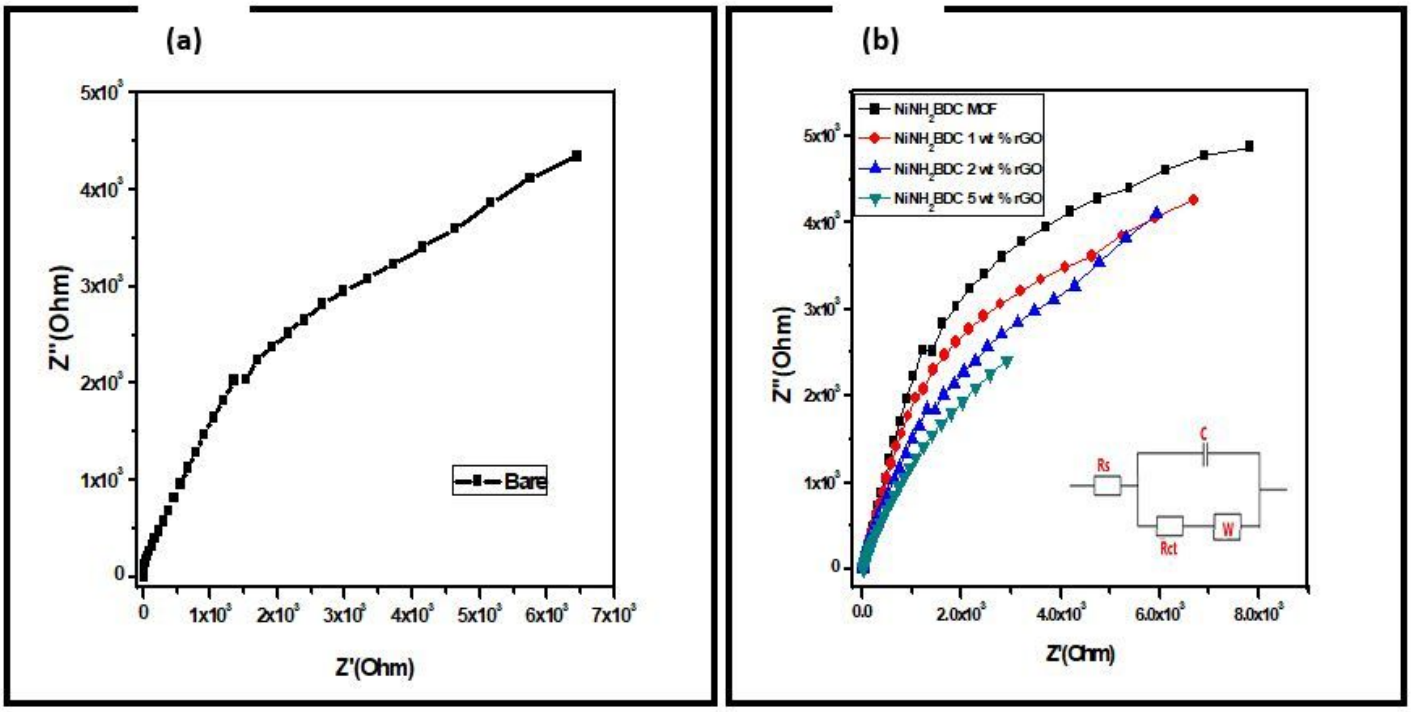

Figure 10

Nyquist plot (a) Bare and (b) NiNH2BDC MOF/1, 2, 5 wt % reduced graphitic carbon hybrids in 3 M CH3OH/1 M NaOH solution at oxidation potential 0.699 V.

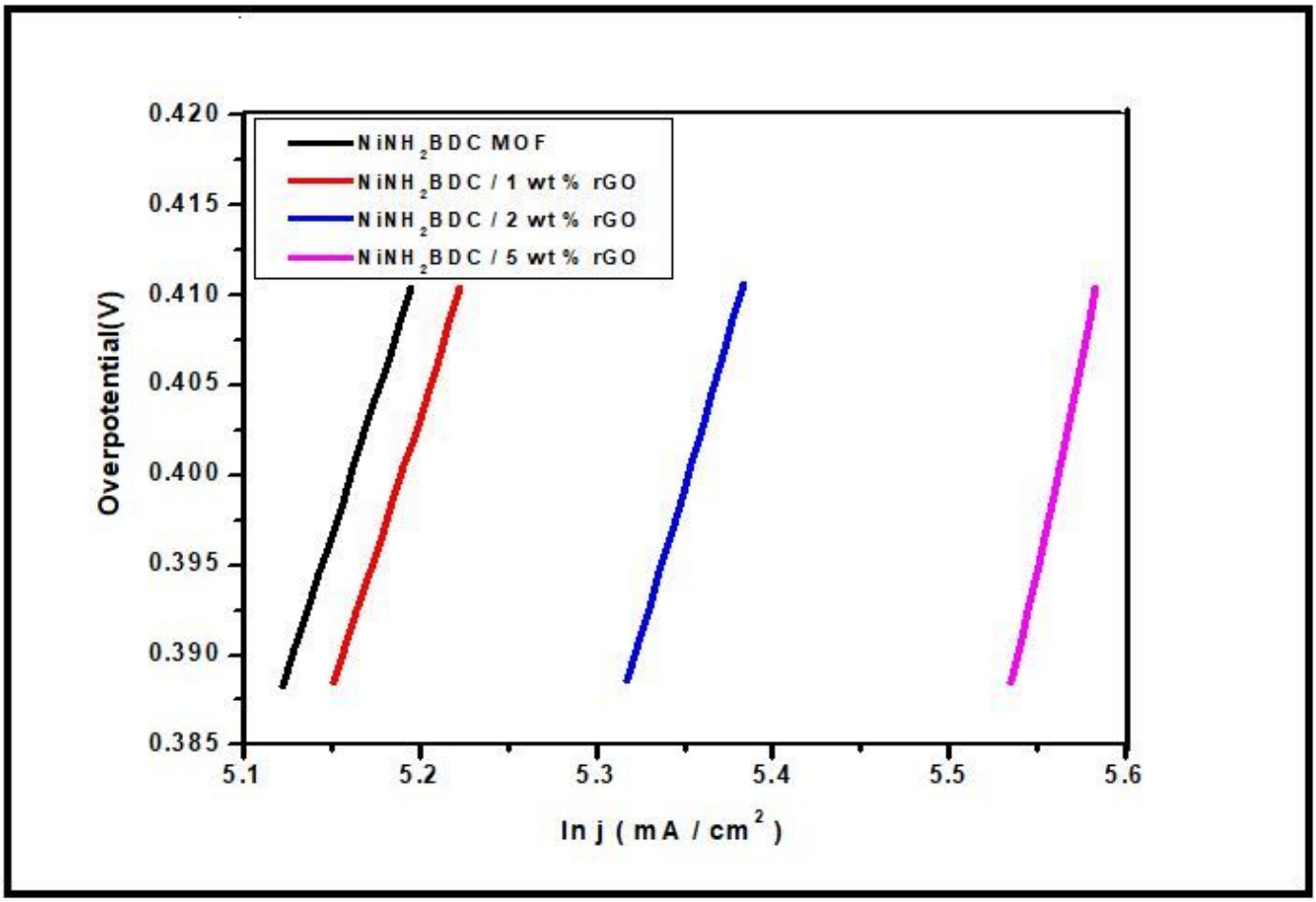

Figure 11

Tafel plot (η vs ln j) of NiNH2BDC MOF/1, 2, 5 wt % reduced graphitic carbon hybrids in 3 M CH3OH/1 M NaOH solution.

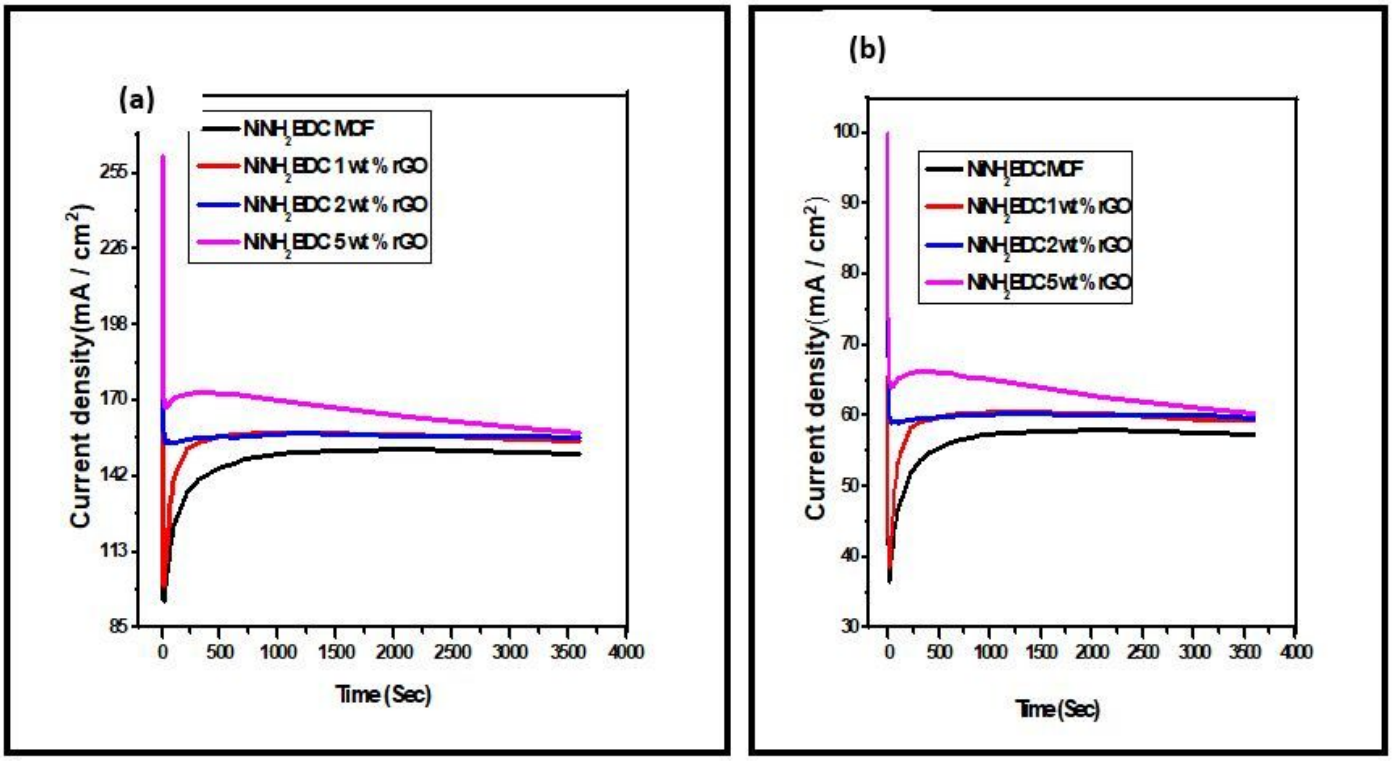

Figure 12

(a) Stability trend of NiNH2BDC MOF/1, 2, 5 wt% reduced graphitic carbon hybrids and (b) % stability retained by samples in 3M CH3OH/1 M NaOH solutions at oxidation potential of 0.69 V vs Hg / HgO for 3600 seconds.

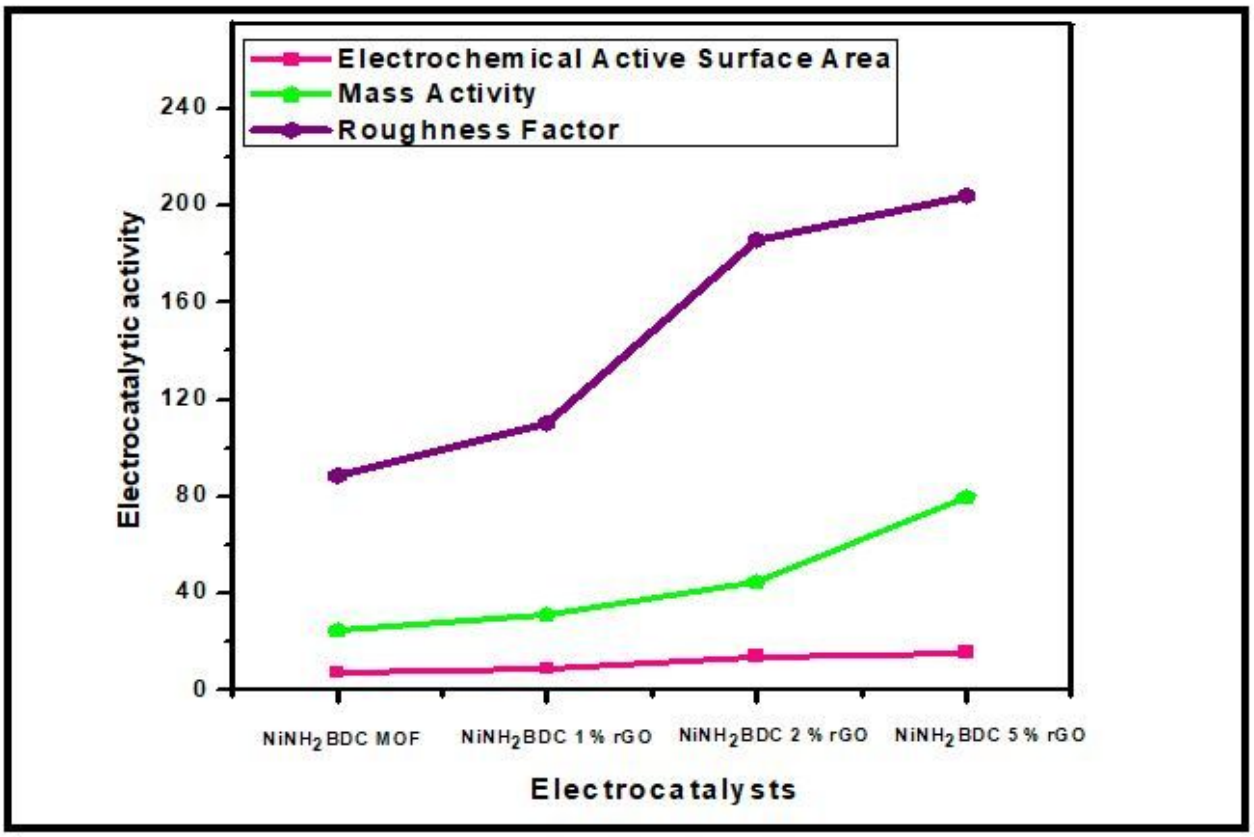

Figure 13

Comparison of EASA, Mass activity, and Roughness factor of NiNH2BDC MOF / 1, 2, 5 wt % reduced graphitic carbon hybrids.

Supplementary Files

This is a list of supplementary files associated with this preprint. Click to download.

- SupplimentryInformationNiNh2BDCrGOMOR.docx